Summer 8-17-2017

CFD Performance of Turbulence Models for Flow from Supersonic Nozzle Exhausts

Han Ju Lee
Washington University in St. Louis

WASHINGTON UNIVERSITY IN ST. LOUIS

School of Engineering and Applied Science

Department of Mechanical Engineering and Materials Science

Thesis Examination Committee:

Ramesh K. Agarwal, Chair

Qiulin Qu

Mark Meacham

CFD Performance of Turbulence Models for Flow from Supersonic Nozzle Exhausts

A Thesis presented to
the School of Engineering &
Applied Science of Washington University in
partial fulfillment of the
requirements for the degree
of Master of Science

August 2017
St. Louis, Missouri

Table of Contents

List of Figures

List of Tables

Acknowledgments

This Master's thesis represents how I have grown to be a scientist and what I have learned through my research experience at Washington University in St. Louis. This place has allowed me to learn and share ideas with one of the most brilliant group of people I have ever known. I would like to use this opportunity to express gratitude to all the people who have guided and supported me throughout 5 years I have spent at Washington University in St. Louis.

First, I would like to thank my advisor, Dr. Agarwal, for his helpful guidance, encouragement and deep knowledge. It would have taken me much longer time and effort to finish this research without him. Moreover, I thank him for making thoughtful comments to improve this manuscript as well. This thesis would have lacked in many ways without him.

Moreover, it was Tim Wray's expertise in ANSYS programs and research methods that gave the momentum to my research. Tim taught me how to use ANSYS programs and solved many problems that I could not have solved. I am also grateful for the long hours he spent to teach me every single detail needed for research, from what to do when certain errors occur to what to check to create a sound mesh. I wish him the best as he starts his scholastic journey this year after finishing PhD under Dr. Agarwal.

Last but not least, I am indebted to my parents for their financial as well as emotional support for my entire academic career. My father's useful advice in deciding which path to follow as well as my mother's heartwarming letters strengthened me to plow through difficult times during my academic career.

Washington University in St. Louis Han Ju Lee

August 2017

Dedicated to my parents, Chang Lyoul Lee and Kyoung Sook Kim.

ABSTRACT OF THE THESIS

CFD Performance of Turbulence Models for Flow from Supersonic Nozzle Exhausts

by

Han Ju Lee

Master of Science in Aerospace Engineering

Washington University in St. Louis, 2017

Research Advisor: Professor Ramesh K. Agarwal

The goal of this thesis is to compare the performance of several eddy-viscosity turbulence models for computing supersonic nozzle exhaust flows. These flows are of relevance in the development of future supersonic transport airplane. Flow simulations of exhaust flows from three supersonic nozzles are computed using ANSYS Fluent. Simulation results are compared to experimental data to assess the performance of various one- and two-equation turbulence models for accurately predicting the supersonic plume flow. One particular turbulence model of interest is the Wray-Agarwal (WA) turbulence model. This is a neat model which has demonstrated promising results mimicking the strength of two equation k-ω model while being a one equation model. Compressibility corrections are implemented for CFD simulations with SST k-ω, k-ε and low Reynolds versions of k-ε models which improved the results compared to the baseline models without compressibility correction. A compressibility correction for WA model is also developed to compare the performance of a compressibility correction to WA model with the compressibility correction to other models. Results show that the standard eddy-viscosity models can capture the shock structure and shear layer of the plume accurately when the thickness of the shear layer is small compared to plume diameter. However, when thickness of the shear layer is relatively large, a compressibility correction should be implemented to predict the supersonic jet

flow. However, the use of compressibility correction consistently overestimates the length of potential core on the centerline of the plume although it improves the prediction of the velocity profile in other regions of the flow field such as the mixing region. Also, it is speculated that an accurate prediction of boundary layer profile at the nozzle exit has an influence in the model's ability to predict the length of potential core as well as the shear layer growth rate. No single model appears to capture all features of the plumes' flow fields without or with compressibility correction. In particular, WA model shows an excellent potential for computation of supersonic nozzles' exhaust flows; however further improvements and investigations in WA model are warranted.

Chapter 1
Introduction

Accurate prediction of engine exhaust plumes from supersonic nozzles using computational fluid dynamics (CFD) software has become a topic of great interest in recent years because of its relevance in the development of future supersonic transport airplanes. This renewed interest in supersonic flight can also be noticed in the outcomes of AIAA Sonic Boom Prediction Workshop [1], where numerous codes have been applied to predict the sonic booms of several model supersonic bodies to test their prediction capability. However, there have been limited investigations of the effect of the engine plume on the boom signature and the supersonic flight vehicle. The goal of this thesis is to partially address this problem by studying the plume flow from supersonic nozzles by numerical simulation. The particular focus is on assessing the performance of several widely used eddy-viscosity turbulence models for computing exhaust flows from supersonic nozzles as well as on developing and evaluating a compressibility correction for the recently developed Wray-Agarwal (WA) turbulence model. The insights gained from this work could perhaps be useful in the simulation of the flow field of the complete supersonic flight vehicles including the engine exhausts.

Flow simulations are conducted using the commercial CFD solver ANSYS Fluent. The three supersonic nozzle exhaust flows for which the experimental data [2, 3, 4] is available are considered. In what follows in rest of the thesis, one of them is referred to as the jet exhaust flow from Putnam nozzle [2], one as an underexpanded jet exhaust flow from Seiner nozzle [3] and the third one as the fully expanded jet exhaust flow from Egger nozzle [4]. Four eddy-viscosity turbulence models are considered: the two-equation k-ε model [5], the two-equation Shear Stress

Transport (SST) k-ω [6] model, the one-equation Spalart-Allmaras (SA) model [7], and the one-equation Wray-Agarwal (WA) model [8]. Three additional low Reynolds number versions of k-ε model by Yang and Shih [9], Launder and Sharma [10], and Abid [11] are also considered for exhaust flow from Seiner nozzle and Eggers nozzle [3]. Compressibility correction of Sarkar et al. [12] is applied to the two-equation k-ε and the three low Reynolds number versions of k-ε model as well as to the WA model to improve the predictions for the underexpanded jet exhaust flow from Seiner nozzle. For WA model, compressibility correction is formed following the approach of Wilcox [13]. Since WA model has been derived from k-ω turbulence model, the compressibility correction for WA model can be easily derived following the derivation of compressibility correction for two-equation k-ω turbulence model [13]. Sarkar et al's compressibility correction [12] has also been implemented for the SST k-ω model [15]. All nozzles, Putnam, Seiner and Eggers are axisymmetric exiting an axisymmetric jet either in a supersonic free stream or in a quiescent freestream. The freestream condition affects the development of the mixing layer and the nature of the mixing layer influences the accuracy of the computations using different turbulence models. Results show that all turbulence models perform quite well without compressibility correction when the thickness of the jet mixing layer is smaller compared to the jet diameter which is the case with the Putnam nozzle. However, compressibility corrections become necessary for accurately computing a thicker mixing layer which is the case with the Seiner nozzle and Eggers nozzle where the flows exhaust into the quiescent freestream, creating a thick shear layer. The results also indicate that an accurate prediction of the boundary layer velocity profile at the nozzle exit is also necessary to capture the supersonic exhaust plume characteristics accurately.

Chapter 2
Turbulence Models

2.1 Shear Stress Transport *k-ω* Model

The SST *k-ω* turbulence model is a two-equation eddy viscosity model combining the best characteristics of the *k-ω* and *k-ε* turbulence models. Near solid boundaries, it behaves like a regular *k-ω* model directly integrable to the wall without repairing additional corrections as is the case with most *k-ε* models. In the free stream and shear layers, its behavior returns to a *k-ε* type model. This avoids strong freestream sensitivity common to *k-ω* type models. The full formulation of the model has been given by Menter [6]. The following equations are the transport equations for *k* and *ω* solved in Fluent in conjunction with the Reynolds Averaged Navier-Stokes (RANS) equations [14].

$$\frac{D\rho k}{Dt} = \tau_{ij}\frac{\partial u_i}{\partial x_j} - \beta^*\rho\omega\kappa + \frac{\partial}{\partial x_j}\left[(\mu + \sigma_k\mu_t)\frac{\partial k}{\partial x_j}\right] \tag{1}$$

$$\frac{D\rho\omega}{Dt} = \frac{\gamma}{\nu_t}\tau_{ij}\frac{\partial u_i}{\partial x_j} - \beta^*\rho\omega^2 + \frac{\partial}{\partial x_j}\left[(\mu + \sigma_\omega\mu_t)\frac{\partial \omega}{\partial x_j}\right] + 2(1-F_1)\rho\sigma_{\omega 2}\frac{1}{\omega}\frac{\partial k}{\partial x_j}\frac{\partial \omega}{\partial x} \tag{2}$$

The turbulent eddy-viscosity is computed from:

$$\nu_t = \frac{k}{\omega \max(\frac{1}{\alpha^*}\omega; \frac{\Omega F_2}{\alpha_1\omega})}\,,\quad \Omega = \sqrt{2W_{ij}W_{ij}}\,,\quad W_{ij} = \frac{1}{2}\left(\frac{\partial u_i}{\partial x_j} - \frac{\partial u_j}{\partial x_i}\right) \tag{3}$$

Each model constant is blended between an inner and outer constant by:

$$\varphi_1 = F_1\varphi_1 + (1-F_1)\varphi_2 \tag{4}$$

The remaining function definitions are given by the following equations:

$$F_1 = tanh(arg_1^4) \tag{5}$$

$$arg_1 = \min\left[\max\left(\frac{\sqrt{k}}{0.09\omega d}, \frac{500\nu}{d^2\omega}\right), \frac{4\rho k}{\sigma_{\omega 2} CD_k d^2}\right] \tag{6}$$

$$\alpha^* = \alpha_0^*\left(\frac{\alpha_0^* + \frac{Re_t}{R_k}}{1 + \frac{Re_t}{R_k}}\right) \tag{7}$$

$$CD_k = \max\left(2\rho\frac{1}{\sigma_{\omega 2}}\frac{1}{\omega}\frac{\partial k}{\partial x_j}\frac{\partial \omega}{\partial x_j}, 10^{-10}\right) \tag{8}$$

$$F_2 = tanh(arg_2^2) \tag{9}$$

$$arg_2 = \max\left(2\frac{\sqrt{k}}{0.09\omega d}, \frac{500\nu}{d^2\omega}\right) \tag{10}$$

The model constants are given in [6].

2.2 Spalart-Allmaras Model

The Spalart-Allmaras (SA) turbulence model is the most commonly used one-equation eddy-viscosity turbulence model. It was derived for application to aerodynamic flows using empiricism and arguments of dimensional analysis. The full formulation of the model is given by Spalart and Allmaras [7]. The following equation is the transport equation for modified eddy viscosity solved in Fluent in conjunction with RANS equations [14].

$$\frac{D\tilde{\nu}}{Dt} = c_{b1}\tilde{S}\tilde{\nu} + \frac{1}{\sigma}\left[\nabla.\left((\nu + \tilde{\nu})\nabla\tilde{\nu}\right) + c_{b2}(\nabla\tilde{\nu})^2\right] - [c_{w1}f_w]\left[\frac{\tilde{\nu}}{d}\right]^2 \tag{11}$$

The turbulent eddy-viscosity is given by the equation:

$$\nu_t = \tilde{\nu} f_{v1}. \tag{12}$$

Near wall blocking is accounted for by the damping function f_{v1}.

$$f_{v1} = \frac{\chi^3}{\chi^3 + c^3{}_{v1}}, \qquad \chi \equiv \frac{\tilde{\nu}}{\nu}. \tag{13}$$

The remaining function definitions are given by the following equations:

$$\tilde{S} \equiv \Omega + \frac{\tilde{\nu}}{\kappa^2 d^2} f_{v2}, \qquad f_{v2} = 1 - \frac{\chi}{1 - \chi f_{v1}} \tag{14}$$

$$f_w = g\left[\frac{1 + c^6{}_{w3}}{g^6 + c^6{}_{w3}}\right]^{1/6}, \tag{15}$$

$$g = r + c_{w2}(r^6 - r), \tag{16}$$

$$r \equiv \frac{\tilde{\nu}}{\tilde{S}\,\kappa^2 d^2}, \tag{17}$$

The model constants are given in [7].

2.3 Wray-Agarwal Model

The Wray-Agarwal (WA) turbulence model is a one-equation eddy-viscosity model derived from *k*-*ω* closure. It has been applied to several canonical cases [8] and has shown improved accuracy over the SA model and competitiveness with the SST *k*-*ω* model. An important distinction between the WA model and previous one-equation *k*-*ω* models is the inclusion of the cross diffusion term in the *ω*-equation and a blending function which allows smooth switching between the two destruction terms. The undamped eddy-viscosity $R = k/\omega$ is determined by:

$$\begin{aligned} \frac{\partial R}{\partial t} + u_j \frac{\partial R}{\partial x_j} = \frac{\partial}{\partial x_j}\left[(\sigma_R R + \nu)\frac{\partial R}{\partial x_j}\right] + C_1 RS + f_1 C_{2k\omega}\frac{R}{S}\frac{\partial R}{\partial x_j}\frac{\partial S}{\partial x_j} \\ - (1 - f_1) C_{2k\varepsilon} R^2 \left(\frac{\frac{\partial S}{\partial x_j}\frac{\partial S}{\partial x_j}}{S^2}\right) \end{aligned} \tag{18}$$

The turbulent eddy-viscosity is given by the equation:

$$\nu_T = f_\mu R \tag{19}$$

The wall blocking effect is accounted for by the damping function f_μ.

$$f_\mu = \frac{\chi^3}{\chi^3 + C_w^3}, \qquad \chi = \frac{R}{\nu} \tag{20}$$

Here *S* is the mean strain given as:

$$S = \sqrt{2S_{ij}S_{ij}}\,, \qquad S_{ij} = \frac{1}{2}\left(\frac{\partial u_i}{\partial x_j} + \frac{\partial u_j}{\partial x_i}\right) \tag{21}$$

While the $C_{2k\omega}$ term is active, Eq. (18) behaves as a one equation model based on the standard *k*-ω equations. The inclusion of the cross diffusion term in the derivation causes the additional $C_{2k\varepsilon}$ term to appear. This term corresponds to the destruction term of one equation models derived from standard *k*-ε closure. The presence of both terms allows the new model to behave either as a one equation *k*-ω or one equation *k*-ε model based on the switching function f_1. The blending function was designed so that the *k*-ω destruction term is active near the solid boundaries and away from the wall near the end of the log-layer the *k*-ε destruction term becomes active. The model constant C_b =1.66 controls the rate at which f_1 switches.

$$f_1 = tanh(arg_1^4) \tag{22}$$

$$arg_1 = \min\left(\frac{C_b R}{S\kappa^2 d^2}, \left(\frac{R+\nu}{\nu}\right)^2\right) \tag{23}$$

The model constants are given in [8].

2.4 Standard *k*-ε Model

The standard *k*-ε model is the first two-equation *k*-ε model published in the turbulence modeling literature and has been extensively applied and modified for computing wide range of industrial flows. This model is included in Fluent [14] as a standard *k*-ε model and employs the wall function for computational efficiency. The transport equation for turbulence kinetic energy *k* is an exact equation while the transport equation for turbulent dissipation (ε) is formulated using physical reasoning. The following are the transport equations for *k* and ε developed by Launder and Spalding [5, 15].

$$\frac{\partial \rho k}{\partial t} + \frac{\partial \rho u_i k}{\partial x_i} = -\rho\overline{u_i u_j}\frac{\partial u_i}{\partial x_i} + \frac{\partial}{\partial x_i}\left[\rho\left(\nu_l + \frac{c_\mu k^2}{\sigma_k \epsilon}\right)\frac{\partial k}{\partial x_i}\right] - \rho\varepsilon \tag{24}$$

$$\frac{\partial \rho \varepsilon}{\partial t} + \frac{\partial \rho u_i \varepsilon}{\partial x_i} = -C_{\varepsilon 1} \rho \overline{u_i u_j} \frac{\partial u_i}{\partial x_i} \frac{\varepsilon}{k} + \frac{\partial}{\partial x_i}\left[\rho\left(\nu_l + \frac{c_\mu k^2}{\sigma_\varepsilon \epsilon}\right)\frac{\partial \varepsilon}{\partial x_i}\right] - C_{\varepsilon 2}\rho\frac{\varepsilon^2}{k} \quad (25)$$

$$\mu_t = \frac{\rho C_\mu k^2}{\varepsilon} \quad (26)$$

The model constants are given in [5].

2.5 Yang-Shih Low Reynolds Number *k-ε* Model

Standard *k-ε* turbulence model described in section 2.4 above employs the wall functions to predict the behavior of flow in proximity of the wall. However, there is no universal wall function that can predict complex flows. The need for more accurate prediction of near wall behavior has resulted in several low Reynolds Number versions of *k-ε* model [9, 10, 11] among several others. The variant of low Reynolds number *k-ε* model described in this section uses a Kolmogorov time scale near the wall to solve the transport equations all the way down to the wall without singularity while behaving like a standard *k-ε* model away from the wall using a damping function [9]. The transport equations for *k* and *ε* are given by:

$$\rho\dot{k} + \rho U_j k_{,j} = \left[\left(\mu + \frac{\mu_T}{\sigma_k}\right)k_{,j}\right]_{,j} - \rho\overline{u_i u_j}U_{i,j} - \rho\varepsilon \quad (27)$$

$$\rho\dot{\varepsilon} + \rho U_j \epsilon_{,j} = \left[\left(\mu + \frac{\mu_T}{\sigma_\epsilon}\right)_{\epsilon,j}\right]_{,j} + \frac{-\rho C_{1\epsilon}\langle u_i u_j\rangle U_{i,j} - C_{2\epsilon}\rho\varepsilon}{T_t} + \rho E \quad (28)$$

The source term *E* in Eq. (28) is given as:

$$\mathrm{E} = \nu\nu_T U_{i,jk} U_{i,jk} \quad (29)$$

This model uses the two time scales, the Kolmogorov time scale near the wall and *k/ε* away from the wall.

$$T_t = \frac{k}{\varepsilon} + T_k \quad (30)$$

$$T_k = c_k\left(\frac{\nu}{\epsilon}\right)^{\frac{1}{2}} \quad (31)$$

The turbulent eddy viscosity is given by the equation:

$$\nu_T = c_\mu f_\mu k T_t \tag{32}$$

where f_μ is the damping function used to account for the wall effect. The damping function is defined as a function of R_y defined as:

$$R_y = \frac{k^{1/2} y}{\nu} \tag{33}$$

The damping function f_μ is defined by:

$$f_\mu = [1 - \exp(-a_1 R_y - a_3 R_y^3 - a_5 R_y^5)]^{1/2} \tag{34}$$

The model constants are given in [9].

Chapter 3
Compressibility Correction

3.1 Compressibility Correction for k-ε Models

A need for compressibility correction has been repeatedly demonstrated after it was first devised by Sarkar et al[12]. Sarkar divides the dissipation, ε, into two components, namely the solenoidal (ε_s) dissipation and the compressible dilatational dissipation (ε_d). He shows that while the solenoidal dissipation remains constant, the dilatational dissipation is heavily affected when turbulent Mach number changes. Thus, Sarkar argues that the dissipation behaves as a function of turbulent Mach number, M_t. Although there is also a pressure dilatation term that directly affects the production of turbulent kinetic energy, k, it has been shown that the main compressibility effect comes from the dilatation dissipation term.

In this thesis, Sarkar's compressibility correction [12] is included in the SST k- ω, k-ε model and the low Reynold number k-ε models of Yang and Shih [9], Abid [11] and Launder & Sharma [10]. Also, a compressibility correction for WA model is derived using the approach for compressibility correction for k- ω model [13]. There are compressibility corrections already employed in some CFD codes. For example, the SST k-ω model in ANSYS Fluent has a built-in compressibility correction term. However, it does not include the entire correction that is given in Ref. [15]. Moreover, turbulence models that approximate the pressure-diffusion and pressure-dilatation terms are relatively few and are not widely used; therefore compressibility correction is generally not included in these models.

As mentioned above, Sarkar's compressibility correction has two parts: dilatation dissipation and the pressure dilatation (PD). It has been shown that these two terms contribute to

the reduction of turbulent kinetic energy in high Mach number flows. The reduction in turbulent kinetic energy decreases the growth rate of shear layer to correctly capture the compressibility effect observed at high Mach numbers. The terms used in the Sarkar's corrections are given below [18]:

$$PD = -\rho\overline{u_i u_j}\frac{\partial u_i}{\partial x_i}(-\alpha_2 M_t^2) + \frac{Re_L}{M_\infty}\,\rho\varepsilon(\alpha_3 M_t^2) \tag{35}$$

$$\Gamma = \alpha_1 M_t^2 \tag{36}$$

$$M_t = \frac{\sqrt{2k}}{a}\ ,\ \ a = \sqrt{\frac{\gamma p}{\rho}} \tag{37}$$

$$\frac{\partial \rho k}{\partial t} + \frac{\partial \rho u_i k}{\partial x_i} = -\rho\overline{u_i u_j}\frac{\partial u_i}{\partial x_i} + \frac{\partial}{\partial x_i}\left[\rho\left(\nu_l + \frac{c_\mu k^2}{\sigma_k \epsilon}\right)\frac{\partial k}{\partial x_i}\right] - \rho\varepsilon(1+\Gamma) + PD \tag{38}$$

$$\frac{\partial \rho\varepsilon}{\partial t} + \frac{\partial \rho u_i \varepsilon}{\partial x_i} = -C_{\varepsilon 1}\rho\overline{u_i u_j}\frac{\partial u_i}{\partial x_i}\frac{\varepsilon}{k} + \frac{\partial}{\partial x_i}\left[\rho\left(\nu_l + \frac{c_\mu k^2}{\sigma_\varepsilon \epsilon}\right)\frac{\partial \varepsilon}{\partial x_i}\right] - f_2 C_{\varepsilon 2}\rho\frac{\varepsilon}{k}\left[\varepsilon - 2\nu_l\left(\frac{\partial\sqrt{k}}{\partial x_i}\right)^2\right] \tag{39}$$

$$f_2 = 1.0 - 0.3\exp\left(-\left(\frac{k^2}{\nu_l \varepsilon}\right)^2\right) \tag{40}$$

Eqs. (38-40) are transport equations for standard *k-ε* model and its turbulent viscosity used in this thesis. The constants in Eqs. (35-37) areα_1, α_2, and α_3; the values of these constants were determined by comparing the calculations with DNS results for compressible turbulence [12]. Although these values of constants perform reasonably well for many flows, the values are not universal and require corrections depending on the type of flow. In this thesis, different values of α_1 have been tested for accurately capturing the mixing layer and potential core of the exhaust. Since the pressure dilatation term has not been shown to have a large influence in compressibility correction, the influence of different values of α_2 and α_3 is not tested. To include the Sarkar's compressibility correction, *PD* and the dilatation dissipation terms are added to the corresponding *k* equations in a turbulence model. As an example, the following equations show the Sarkar's compressibility correction applied to a low Reynolds version of *k-ε* model [18].

In eqns. (41)-(43), pressure dilatation term *PD* and dilation dissipation term Γ are added to *k* transport equation of Launder and Sharma model [10] to include the Sarkar's compressibility correction. The following equations show the Sarkar's compressibility correction applied to Launder and Sharma low Reynolds number *k-ε* model.

$$\frac{\partial \rho k}{\partial t}+\frac{\partial \rho u_i k}{\partial x_i}=-\rho\overline{u_i u_j}\frac{\partial u_i}{\partial x_i}+\frac{\partial}{\partial x_i}\left[\rho\left(\nu_l+\frac{c_\mu k^2}{\sigma_k \epsilon}\right)\frac{\partial k}{\partial x_i}\right]-\rho\varepsilon(1+\Gamma)+PD - 2\nu_l\left(\frac{\partial\sqrt{k}}{\partial x_i}\right)^2 \tag{41}$$

$$\frac{\partial \rho \varepsilon}{\partial t}+\frac{\partial \rho u_i \varepsilon}{\partial x_i}=-C_{\varepsilon 1}\rho\overline{u_i u_j}\frac{\partial u_i}{\partial x_i}\frac{\varepsilon}{k}+\frac{\partial}{\partial x_i}\left[\rho\left(\nu_l+\frac{c_\mu k^2}{\sigma_\varepsilon \epsilon}\right)\frac{\partial \varepsilon}{\partial x_i}\right]-f_2 C_{\varepsilon 2}\rho\frac{\varepsilon^2}{k}+E \tag{42}$$

$$E=\nu\nu_t\left(\frac{\partial^2 U}{\partial y^2}\right)^2 \tag{43}$$

3.2 Compressibility Correction for SST *k-ω* model

For SST *k-ω* turbulence model, the transport equations with compressibility corrections have been derived by Suzen and Hoffman [15]. They start with Jones Launder *k-ε* model with compressibility correction applied in the same manner as described in Eqns. (38-40). From Jones-Lounder *k-ε* model, following Mentor's derivation of SST *k-ω* model from standard *k-ε* model, they derive the SST *k-ω* model with compressibility correction as shown in Eqns. (44) and (45).

$$\frac{\partial \rho k}{\partial t}+\frac{\partial \rho u_i k}{\partial x_i}=-\rho\overline{u_i u_j}\frac{\partial u_i}{\partial x_i}-\rho\omega\beta^* k[1+\alpha_1 M_t^2(1-F_1)]+(1-F_1)PD + \frac{\partial}{\partial x_i}\left[(\mu+\sigma_k\mu_t)\frac{\partial k}{\partial x_i}\right] \tag{44}$$

$$\frac{\partial \rho w}{\partial t}+\frac{\partial \rho u_i \omega}{\partial x_i}=-\rho\overline{u_i u_j}\frac{\partial u_i}{\partial x_i}\frac{\gamma}{\nu_t}-(1-F_1)\frac{PD}{\nu_t}-\beta\rho\omega^2+(1+F_1)\beta^*\alpha_1 M_t^2\rho\omega^2 + 2\rho\sigma_{\omega 2}\frac{1}{\omega}(1-F_1)\frac{\partial k}{\partial x_i}\frac{\partial \omega}{\partial x_i}+\frac{\partial}{\partial x_i}\left[(\mu+\sigma_\omega\mu_t)\frac{\partial \omega}{\partial x_i}\right] \tag{45}$$

3.3 Compressibility Correction for WA Model

The method used to derive the WA model from Wilcox *k-ω* model by Wray and Agarwal is used to obtain the compressibility correction for WA model following the approach of Wilcox [13] in deriving the compressibility correction for *k-ω* model. To apply the compressibility terms to *k-ω* model, Wilcox modified the closure coefficients β and β^* to vary with M_t as shown in Eqns. (46-47). The compressibility function can be switched to either Sarkar's [12] or Wilcox's [13] and are shown in Eqns. (48-49).

$$\beta = \beta_0 - \beta_0^* F(M_t) \tag{46}$$

$$\beta^* = \beta_0^* [1 + \xi^* F(M_t) \tag{47}$$

$$\text{Sarkar}: \quad \xi^* = 1, \quad F(M_t) = M_t^2 \tag{48}$$

$$\text{Wilcox}: \quad \xi^* = \frac{3}{2}, \quad M_{t0} = \frac{1}{4}, \quad \mathrm{F}(M_t) = [M_t^2 - M_{t0}^2] H(M_t - M_{t0}) \tag{49}$$

With *R* defined as *k/ ω* in WA model, the substantial derivative can be obtained as [8]:

$$\frac{\mathrm{D}R}{\mathrm{Dt}} = \frac{1}{\omega}\frac{\mathrm{D}k}{\mathrm{Dt}} - \frac{k}{\omega^2}\frac{\mathrm{D}\omega}{\mathrm{D}t} \tag{50}$$

Bradshaw's Relation is defined as:

$$\left|-\overline{\acute{u}\acute{v}}\right| = \nu_t \left|\frac{\partial u}{\partial y}\right| = a_1 k \tag{51}$$

With substitution of *k* and *ω* from Wilcox [13] transport equations for *k* and *ω* in Eq. (50) transport equations and employing the of Bradshaw's relation (51) to relate the turbulent kinetic energy and turbulent shear stress, the *R* equation can be obtained as shown in Eq. (52). The coefficients in rectangle in front of the production term of the standard WA equation were calibrated by computing the canonical cases in paper by Wray and Agarwal [8]. It is important to note the inclusion of closure coefficients β and β^* from Wilcox *k-ω* model in the production term

of WA equation. The only term that contains β and β^* is the production term while the destruction terms and the diffusion term remain unchanged from the original WA equation. Therefore, as was the case in compressibility correction for *k-ω* model by Wilcox, β and β^* in *R* equation can be switched according to Eq. (46-47) to obtain a compressibility correction. The compressibility corrected form of WA equation is shown in Eq. (53) where $F(M_t)$ is the two types of compressibility correction functions given in Eq. (48) and Eq. (49). In this thesis, the compressibility correction of Sarkar et al. [12] and Wilcox [13] are employed. Different values of compressibility coefficients, C_{Comp} , are tested to obtain the best results when compared against the experimental data.

$$\frac{\mathrm{D}R}{\mathrm{D}t} = \boxed{\left(a_1 + \frac{\beta^* f_\mu}{a_1} + \frac{\beta f_\mu}{a_1} - \alpha a_1\right)} RS + \frac{\partial}{\partial \mathrm{y}}\left(\sigma_R R \frac{\partial R}{\partial y}\right) + f_1 C_{2k\omega} \frac{R}{S}\frac{\partial R}{\partial x_j}\frac{\partial S}{\partial x_j} - (1 - f_1) C_{2k\varepsilon} R^2 \left(\frac{\frac{\partial S}{\partial x_j}\frac{\partial S}{\partial x_j}}{S^2}\right) \tag{52}$$

$$\frac{\mathrm{D}R}{\mathrm{D}t} = -C_{comp} F(M_t)\mathrm{RS} + C_1 RS + \frac{\partial}{\partial \mathrm{y}}\left(\sigma_R R \frac{\partial R}{\partial y}\right) + f_1 C_{2k\omega} \frac{R}{S}\frac{\partial R}{\partial x_j}\frac{\partial S}{\partial x_j} - (1 - f_1) C_{2k\varepsilon} R^2 \left(\frac{\frac{\partial S}{\partial x_j}\frac{\partial S}{\partial x_j}}{S^2}\right) \tag{53}$$

Since the definition of M_t contains turbulent kinetic energy, *k*, a treatment to change *k* into a usable form in *R* equation is needed. We utilize a modified Bradshaw relation to relate *k* and *R*. The original Bradshaw can also be used. However, as will be shown later, capturing the boundary layer profile is important in the prediction of supersonic exhaust with shear layer, therefore the modified Bradshaw relation is used here to improve the capturing of the boundary layer effect. The modified Bradshaw relation [19] is defined as follows:

$$M_t = \frac{\sqrt{2k}}{a} \; where \; k = \sqrt{\tilde{k}^2 + k_\alpha^2} \tag{54}$$

$$\tilde{k} = \frac{f_\mu R}{a_1}\left|\frac{\partial u}{\partial y}\right| \tag{55}$$

$$k_\alpha = \nu S_\alpha \tag{56}$$

$$S_\alpha = \frac{2C_\alpha f_\alpha}{3\nu}\left(\frac{\sqrt{\frac{u_i^2}{2}}}{1+\frac{\mu_T}{\mu}}\right)^2 \tag{57}$$

$$C_\alpha = \sqrt{C_\mu^2 + \frac{\nu}{R+\nu}} \quad , \qquad f_\alpha = 1 - \exp\left(-\frac{\mu_T}{36\mu}\right) \tag{58}$$

Chapter 4
Supersonic Nozzle Exhaust Test Cases

4.1 Putnam Nozzle

The first test case considered corresponds to the experiment of Putnam and Capone [2]. The Putnam nozzle geometry is obtained from a report by Putnam. The data was generated at the NASA LaRC 4x4 foot supersonic tunnel. The case is run at a freestream Mach number of 2.2, Reynolds number of 1.86×10^6 based on the model maximum diameter of 15.24 cm, and Nozzle Pressure Ratio (NPR) of 8.12. "Nozzle 6" of Ref. [2] is used in this study. Figure 1 shows the nozzle geometry. CFD analysis of the Putnam nozzle is performed at free stream Mach number of 2.2, total temperature of 312K and NPR of 8.12. Flow conditions at the nozzle inlet are calculated using the isentropic relations with inlet Mach number of 0.3. At the inlet, boundary condition are set as a total pressure of 9.92×10^5 Pa, static pressure of 8.85×10^4 Pa, and total temperature of 553 R. Jet exit is set as x = 0.

4.2 Seiner Nozzle

The second case considered corresponds to the experiment of Seiner et al. [3]. The geometry of the Seiner nozzle is obtained from open source by NASA [3]. The data for the nozzle was obtained for a jet exit Mach number M=2.0. The Reynolds number based on the jet exit diameter is Re $=1.3 \times 10^6$. The jet from this nozzle is discharged into a near quiescent freestream. Figure 2 shows the nozzle geometry. Boundary conditions at the nozzle inlet are total pressure of 7.03×10^5 Pa, NPR of 7.82, Mach number of 0.3, and static temperature of 300K. The freestream boundary condition is set at standard atmospheric pressure and room temperature. Jet exit is set as x = 0 along the centerline.

4.3 Eggers Nozzle

The final case tested corresponds to the experiment of Eggers [4]. This axisymmetric supersonic nozzle discharges a perfectly expanded isothermal free jet at Mach 2.22 with NPR of 11. The jet from this nozzle is discharged into a near quiescent freestream as well. Figure 3 shows the nozzle geometry. Boundary conditions for the nozzle inlet are Mach number of 0.3 and static temperature of 291K. Free stream boundary condition was set at standard atmospheric pressure and room temperature. Nozzle throat is set as x=0 along the centerline. For evaluation of simulation results, experimental velocity data normalized by exit velocity at the centerline is used. Table 1 tabulates the internal coordinates for geometry of the nozzle.

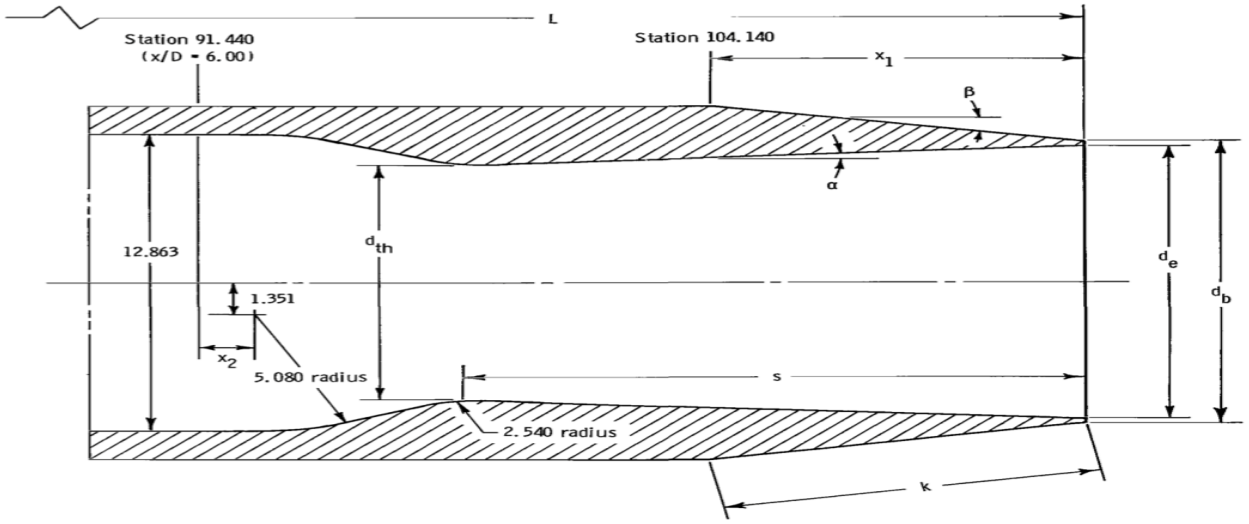

Nozzle	$M_{j,des}$	$\left(p_{t,j}/p_{\infty}\right)_{des}$	α, deg	β, deg	x_1	L	k	s	d_{th}	d_e	d_b	A_{th}	A_e	A_e/A_{th}	x_2
6	2.024	8.12	6.04	5	9.109	113.249	9.144	15.105	10.223	13.417	13.646	82.08	141.39	1.722	1.778

Details of nozzles. All dimensions are in centimeters except as noted. Areas listed are in square centimeters.

Fig. 1 Putnam nozzle geometry from Ref. [2].

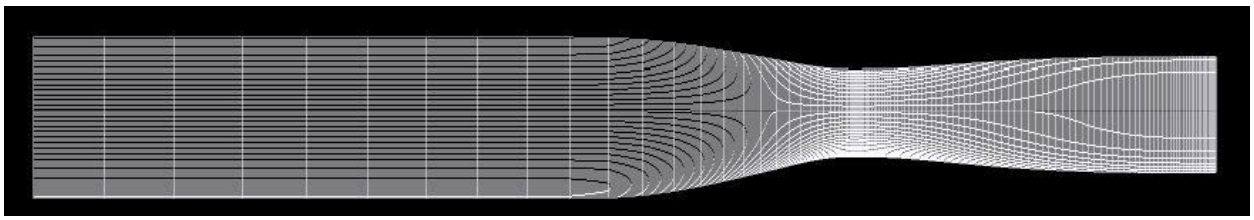

Fig. 2: Seiner nozzle geometry from Ref. [16].

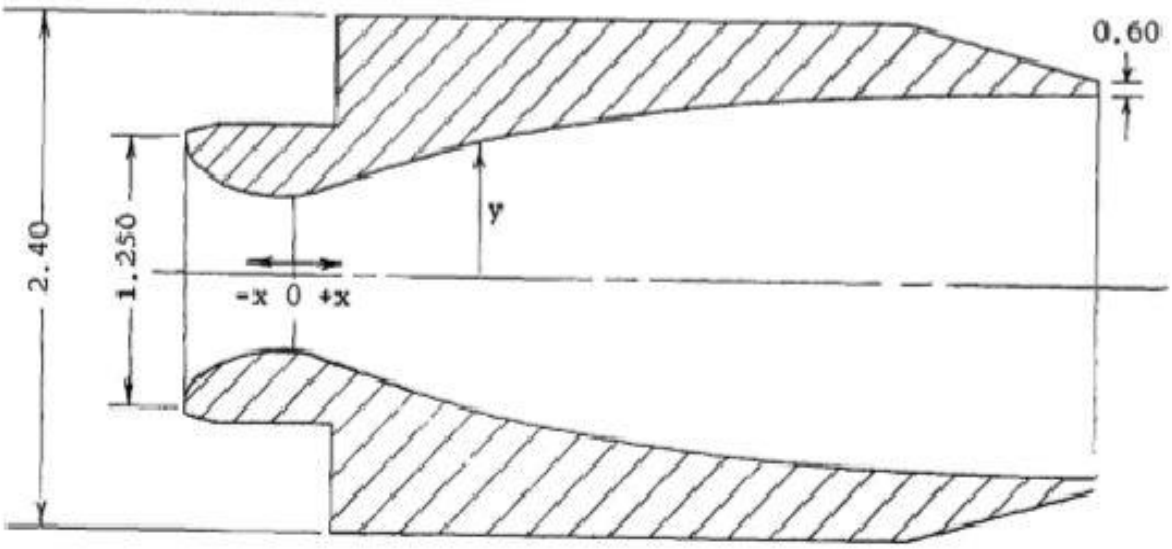

Figure 3 Eggers nozzle geometry from Ref. [20]

Table 1 Nozzle internal coordinates for Eggers nozzle [20]

x (in)	r (in)
-.5230	.6250
-.5200	.5469
-.4900	.5080
-.4500	.4724
-.3000	.3987
-.1500	.3640
0.0000	.3535
.0354	.3570
.0707	.3623
.1414	.3747
.2828	.3995
.4242	.4242
.5656	.4461
.7070	.4638
.9191	.4850
1.1312	.4977
1.3433	.5027
1.5625	.5041

Chapter 5
Results and Discussion

5.1 Grid Generation, Solver Specification and Convergence

The mesh generation software ANSYS ICEM is used to construct the computational domain and mesh. Grids for Putnam, Seiner and Eggers nozzle are shown in figures 4, 5 and 6, respectively. An adaptive grid feature in ANSYS Fluent based on density gradients is utilized for meshing the computational domain. This method assumes that the maximum error occurs in the maximum gradient region. Therefore, a converged solution with a lower number of cells is obtained at first for the adaptive grid algorithm in ANSYS Fluent to recognize the high gradient region so that more cells can be added in the region of interest e.g. a shear layer region. Figures 4, 5 and 6 show the original and adapted grids for the Putnam nozzle, the Seiner nozzle and the Eggers nozzle, respectively. The Figures show that the adaptive grid algorithm in ANSYS Fluent creates more cells in regions of interest e.g. in the shock cell and shear layer regions. The final number of cells in the mesh for Putnam nozzle is 8.99×10^5. The final number of cells in the mesh for Seiner nozzle is 2.09×10^5. The final number of cells in the mesh for Eggers Nozzle is 2.36×10^5. For all cases, second order upwind scheme is used. SST k-ω model is also run with a third order MUCSL scheme. However, no noticeable difference between the results from second order and the third order schemes is observed. The initial convergence criteria for various residuals is set at 1×10^{-6}. However, the residual values many times did not reach a value of 10^{-6}, therefore the solution was determined converged when the drag coefficient on the wall became constant over a large number of iterations.

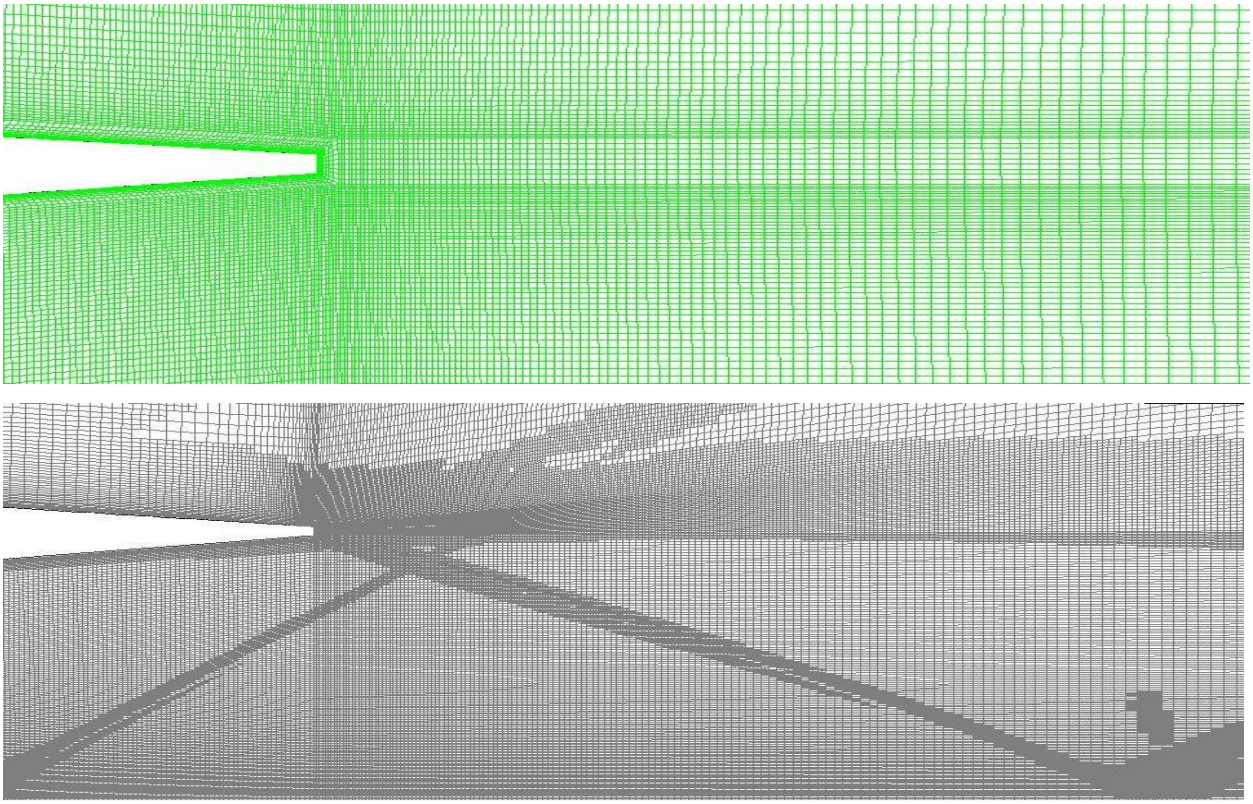

Figure 4 Original and adapted grids for the Putnam nozzle.

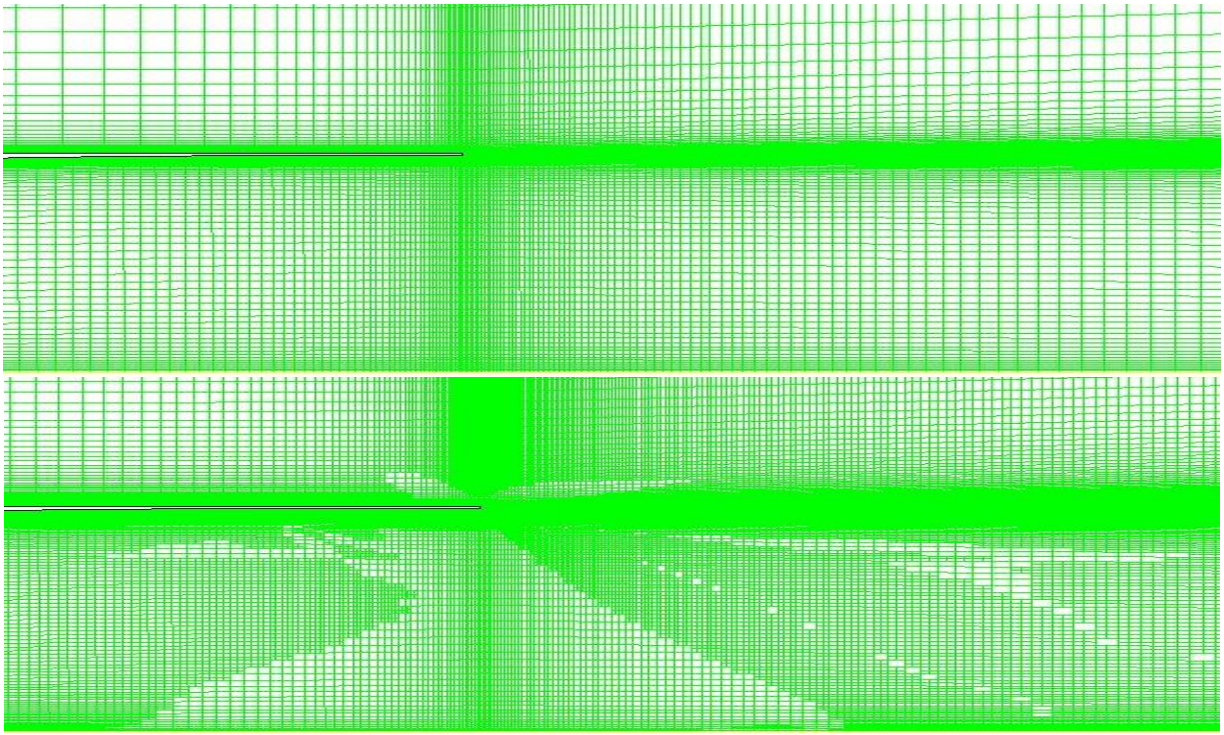

Figure 5 Original and adapted grids for the Seiner nozzle.

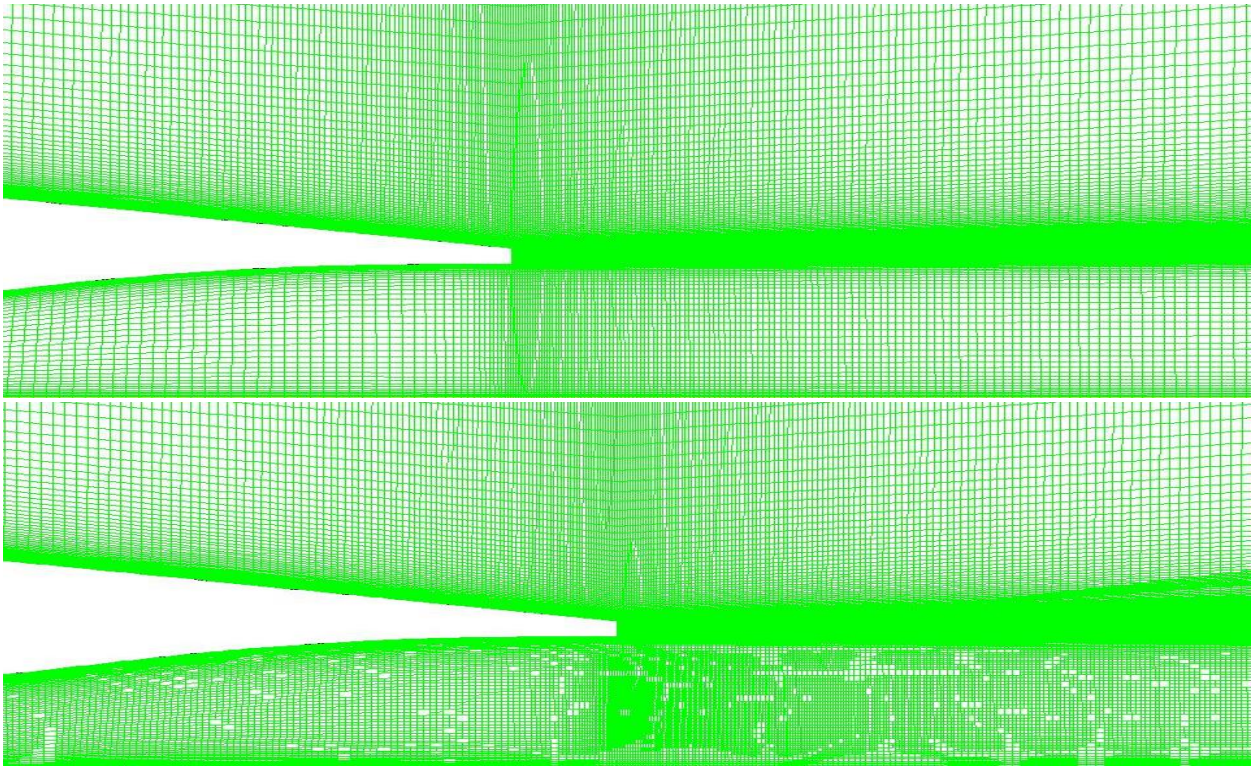

Figure 6 Original and Adapted grids for Eggers Nozzle

5.2 Putnam Nozzle Results

In case of Putnam nozzle, the freestream Mach number is close to the Mach number at the jet exhaust, therefore this case does not exhibit a strong thick mixing layer. Variation in computed $\Delta P/P_0$ and Mach number profiles at 15.24cm above the centerline of the nozzle are compared with the experimental data in Fig. 7 and Fig. 8 respectively using the standard k-ε, SA, SST k-ω models with and without compressibility correction, and the WA model without compressibility correction. All models capture the shock structure quite well. $\Delta P/P_0$ and Mach number profiles from the simulation also agree very well with the experimental results. Figures 9 and 10 show the Mach number contours in the Putnam nozzle exhaust obtained with the SST k-ω model. Figures 11 and 12 show the static pressure contours in the Putnam nozzle exhaust obtained with the SST k-ω model.

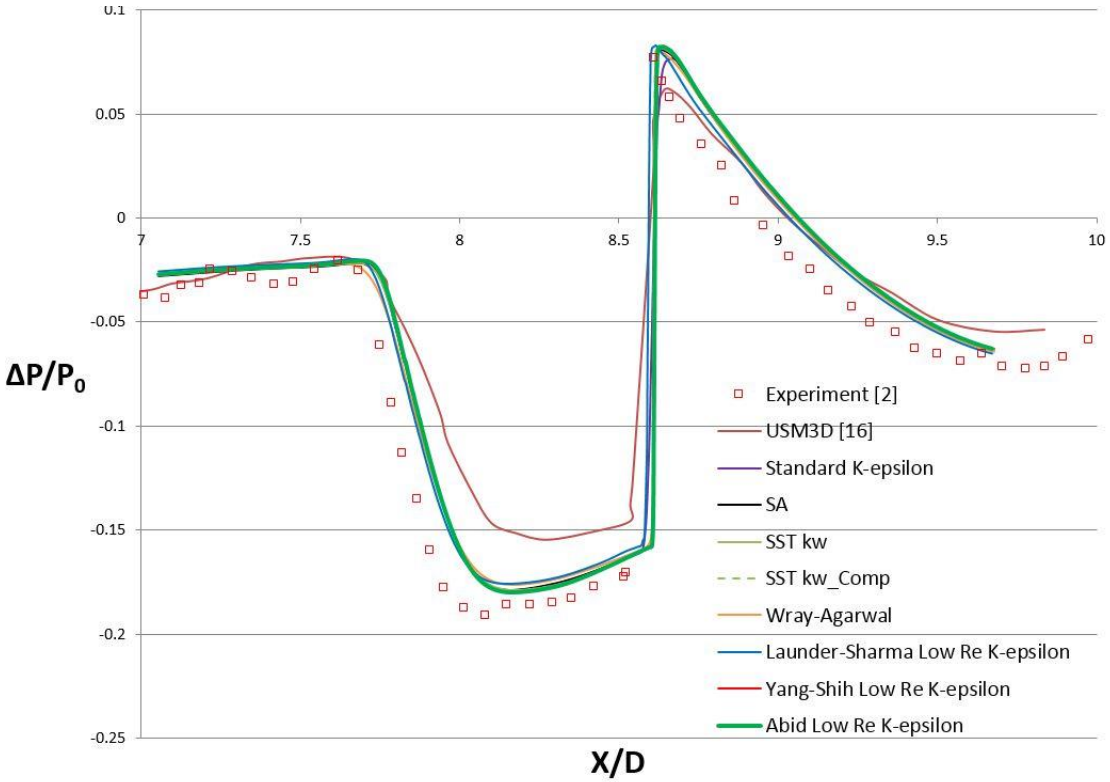

Figure 7 Variation in Pressure ΔP/P0 along the axis at a distance 15.24 cm above the centerline of Putnam nozzle.

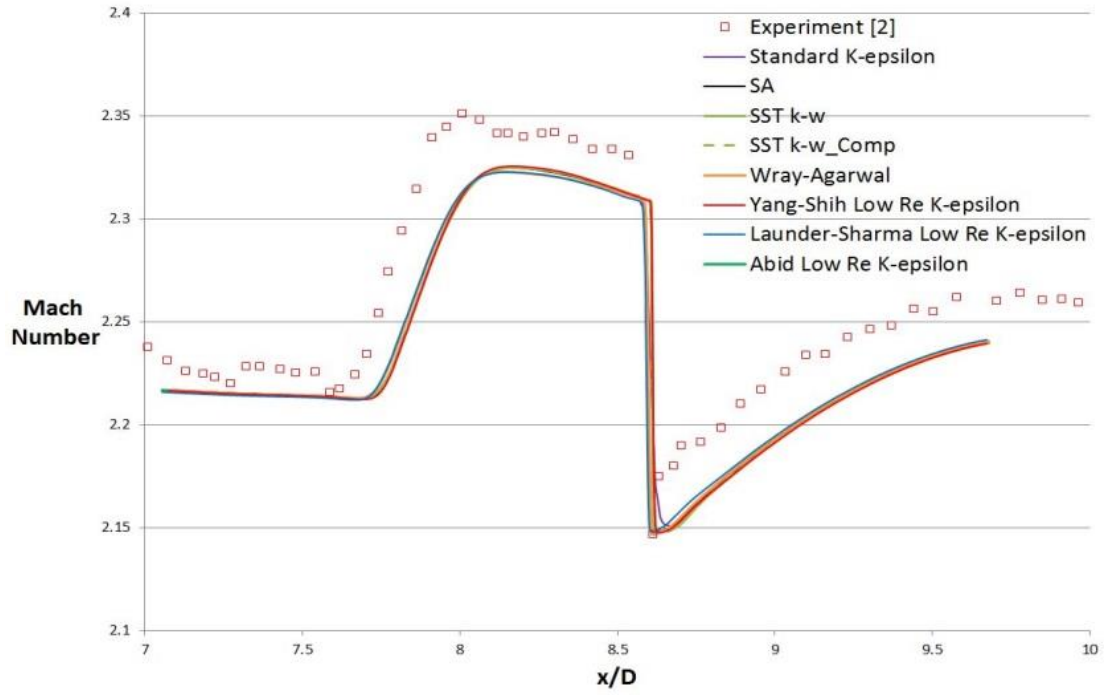

Figure 8 Variation in Mach number along the axis at a distance 15.24 cm above the centerline of Putnam nozzle.

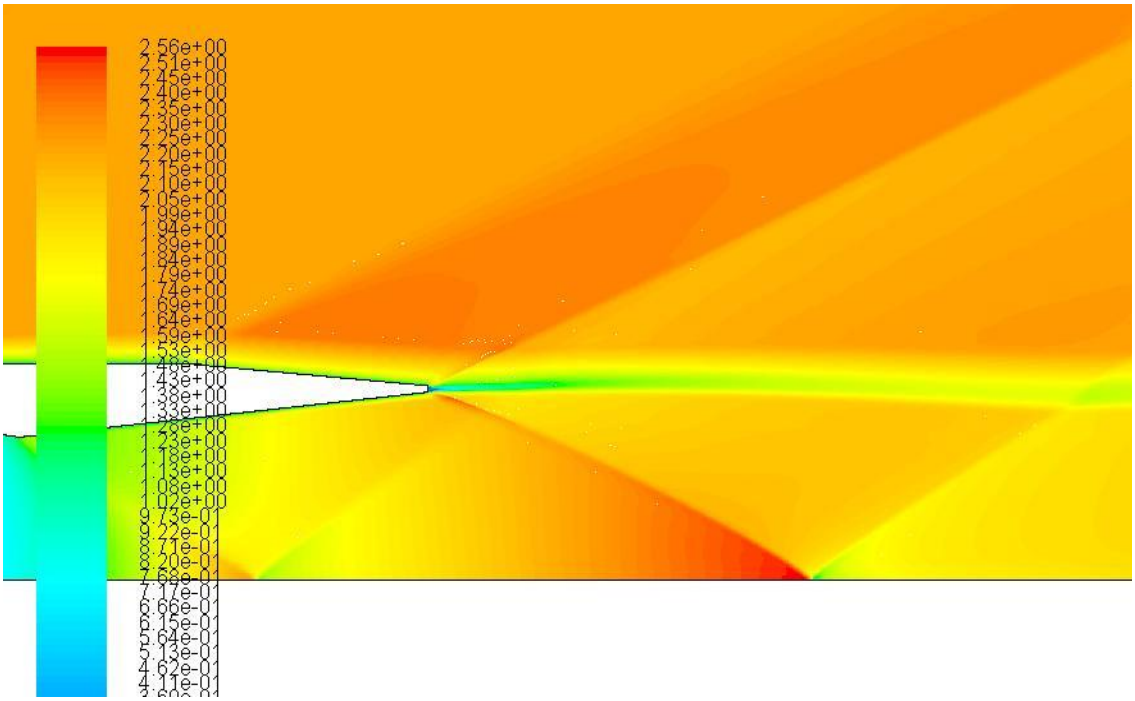

Figure 9 Mach contours in Putnam nozzle exhaust using the SST *k-ω* model.

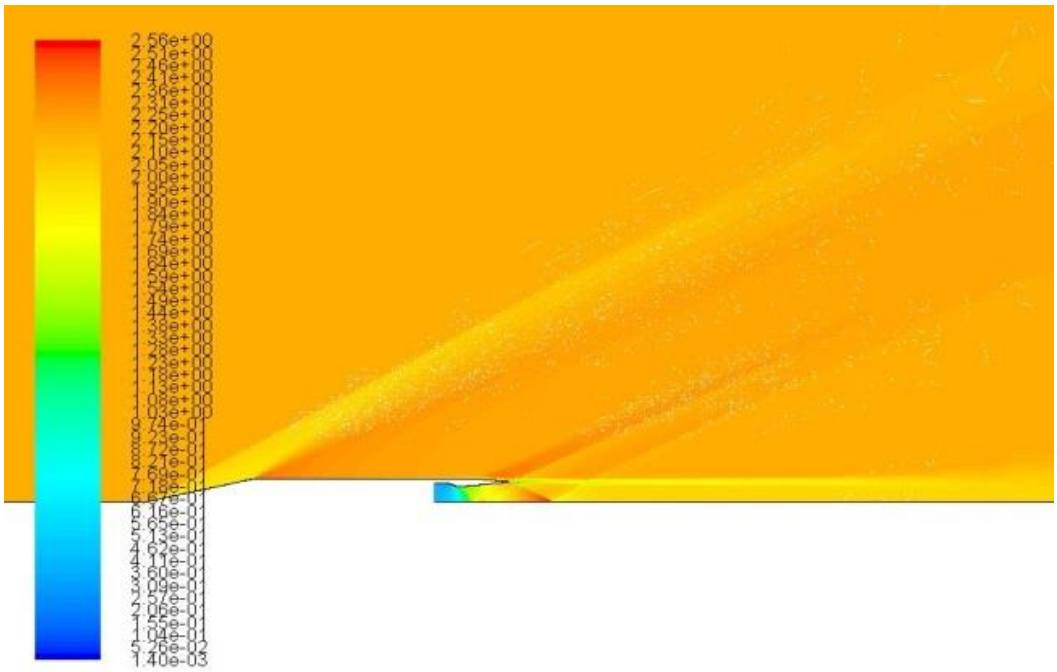

Figure 10 Zoomed-in Mach contours in Putnam nozzle exhaust using SST *k-ω* model.

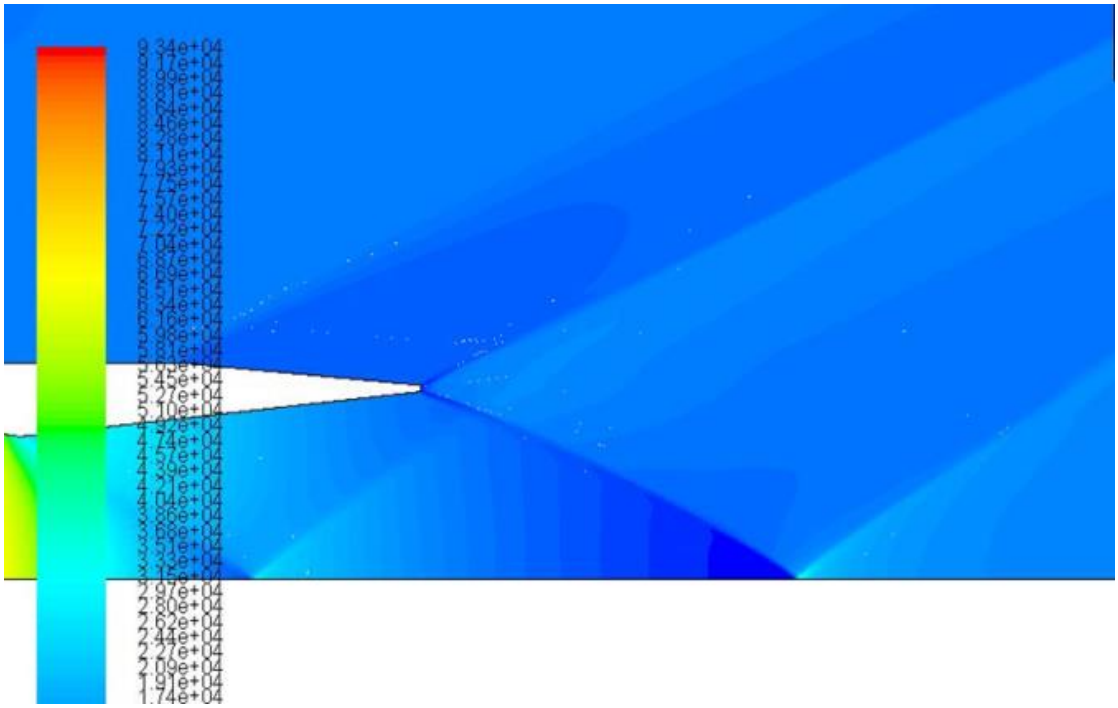

Figure 11 Pressure contours in Putnam nozzle exhaust using SST *k-ω* model.

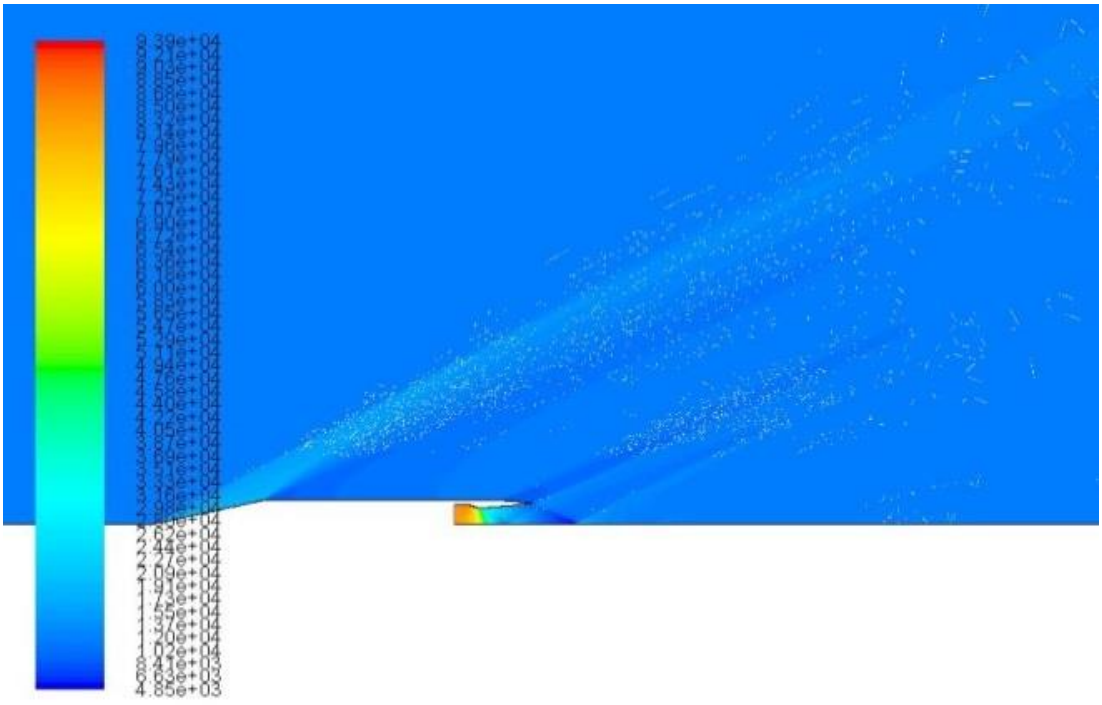

Figure 12 Zoomed-in pressure contours in Putnam nozzle exhaust using SST *k-ω* model.

5.3 Seiner Nozzle Results

5.3.1 Results without Compressibility Correction

CFD simulations for Seiner nozzle are conducted with SA model, SST k-ω model with and without compressibility correction, the standard k-ε model with and without compressibility correction, low Reynolds number k-ε models of Yang and Shih, Abid, and Launder and Sharma with and without compressibility correction and the Wray-Agarwal(WA) model with and without compressibility correction.

The baseline turbulence models without compressibility correction, namely the SST k-ω, standard k-ε, Wray-Agarwal and SA model results are compared with the experimental data in Fig. 13. Although all the baseline turbulence models except the WA model show the expected oscillatory behavior in the exhaust plume, Fig. 13 shows that the standard turbulence models in ANSYS Fluent fail to capture the strength and location of the internal shock structure of the exhaust plume from the Seiner nozzle. It should be noted that the WA model correctly captures the peak location of the shock oscillation although not the amplitude. However, the strength of the shock structure in the exhaust plume is completely different compared to all other baseline models. The baseline models show faster shear layer growth rate causing the Mach number to drop faster than the experimental data. This behavior is expected since the baseline models do not include the compressibility effects. To allow for slow growth rate of shear layer, compressibility correction is needed since it inhibits the shear layer growth rate. Therefore, Sarkar's compressibility correction [12] is applied to the baseline models to accurately capture the shear layer growth observed in the experimental data. Figures 14 and 15 show the Mach number contours in the Seiner nozzle exhaust obtained with the SST k-ω model. Figures 16 and

17 show the static pressure contours in the Seiner nozzle exhaust obtained with the SST *k-ω* model.

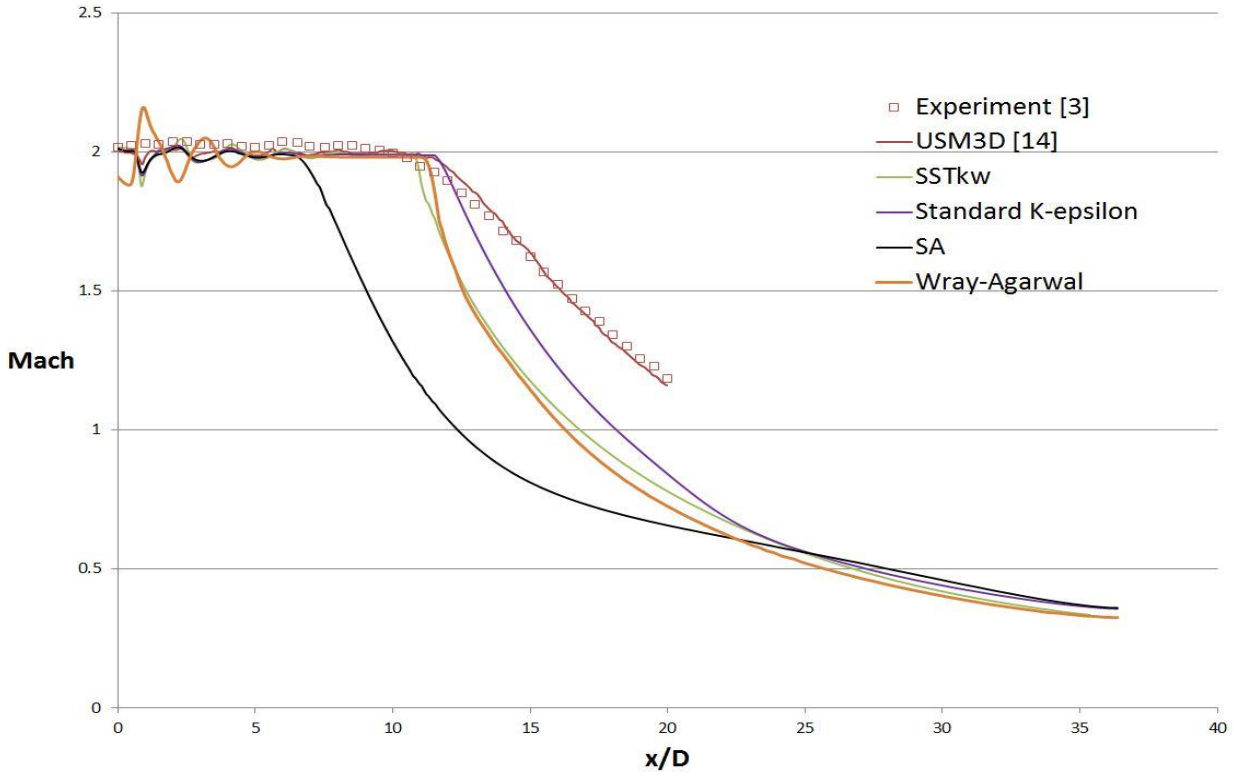

Figure 13 Variation in Mach number along the centerline from the jet exit for Seiner nozzle using various standard baseline turbulence models.

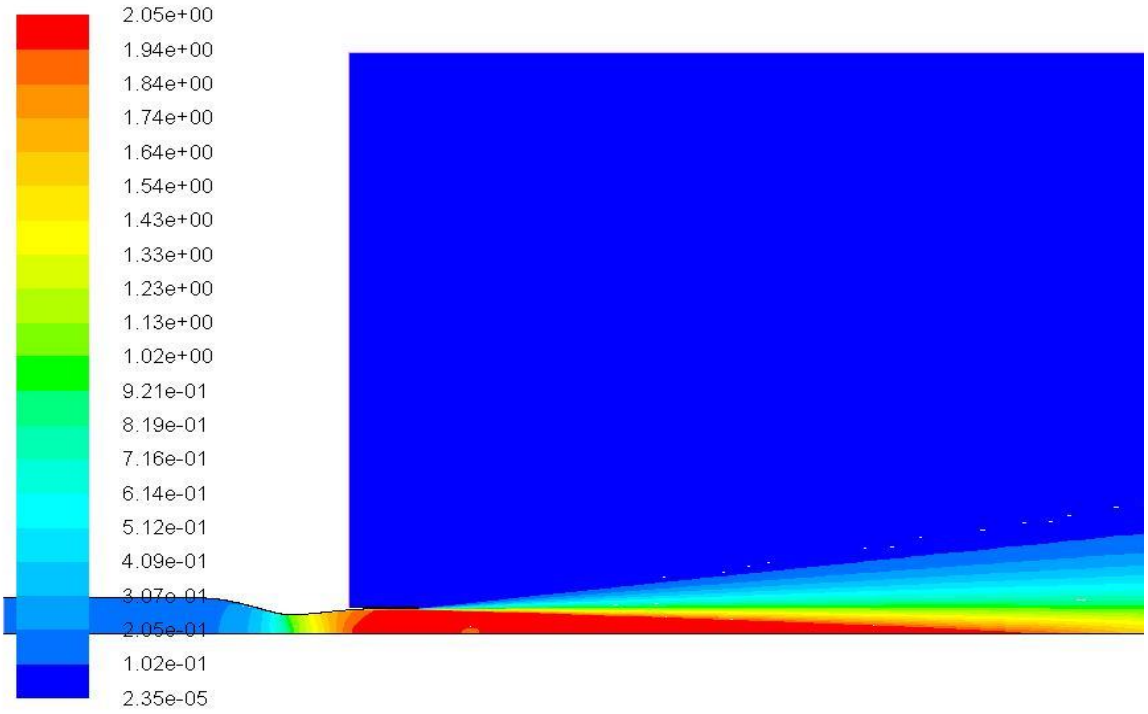

Figure 14 Mach contours in Seiner nozzle exhaust using SST *k-w* model.

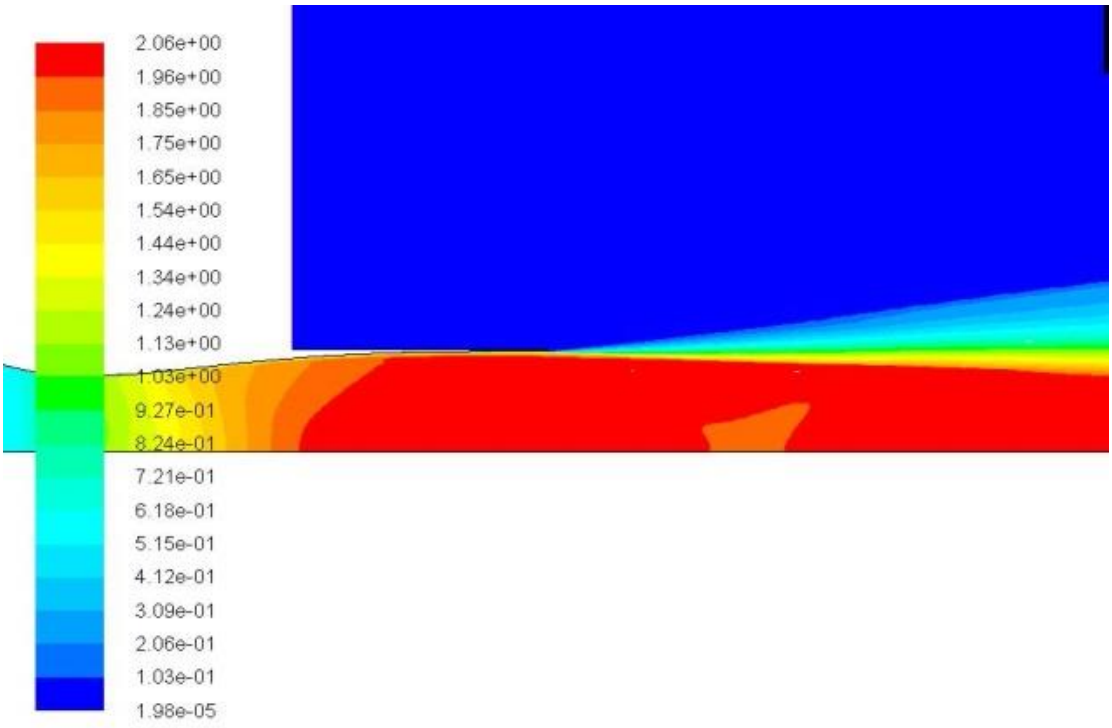

Figure 15 Zoomed-in Mach contours in Seiner nozzle exhaust using SST *k-w* model.

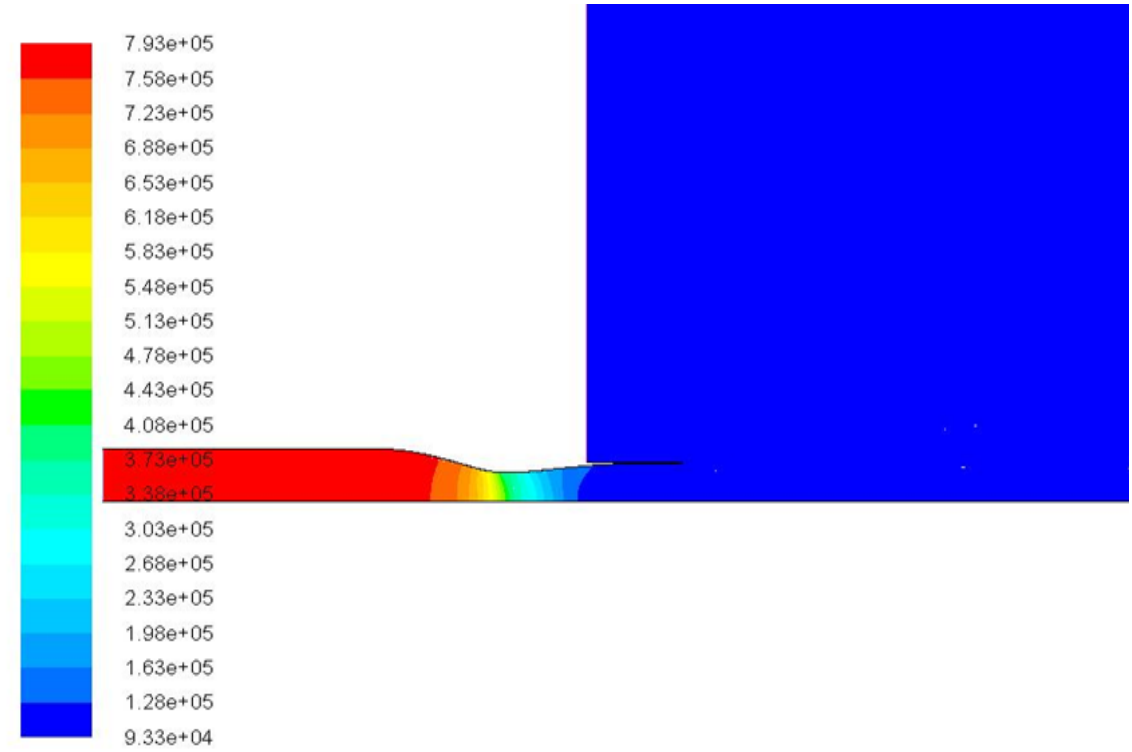

Figure 16 Pressure contours in Seiner nozzle exhaust using SST *k-w* model.

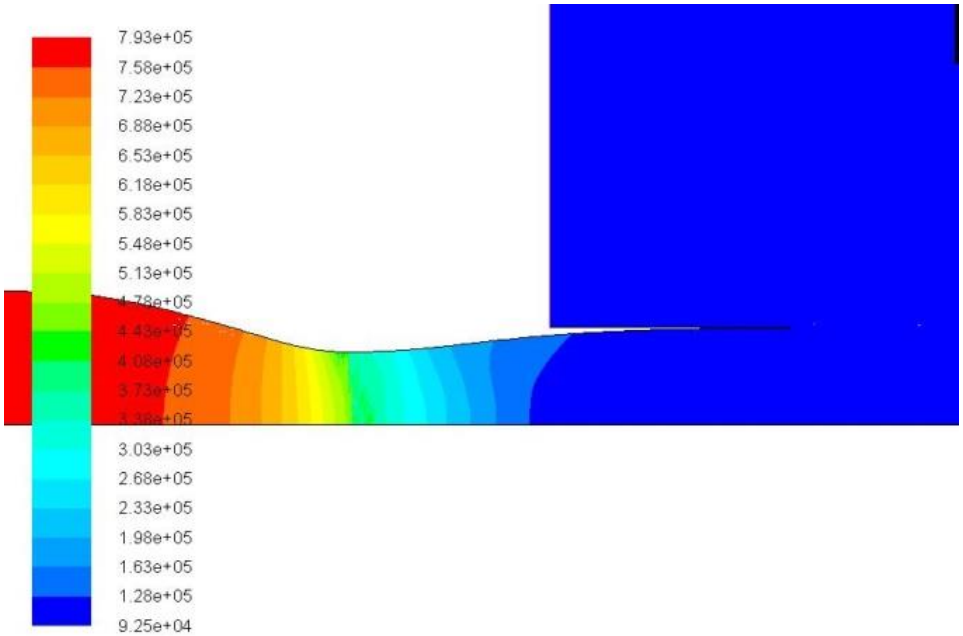

Figure 17 Zoomed-in pressure contours in Seiner nozzle exhaust using SST *k-w* model.

5.3.2 Results with Compressibility Correction for *k-ε* and SST *k-ω* Models

Simulations for Seiner nozzle are conducted with standard *k-ε* model with compressibility correction, the SST *k-ω* model with compressibility correction, and the Yang - Shih low Reynolds number *k-ε* model with and without compressibility correction. Figure 18 compares the results obtained from each turbulence model. SST *k-ω* model with compressibility correction fails to match the experimental data. The *k-ε* model with compressibility correction and Yang-Shih low Reynolds number *k-ε* model with and without compressibility correction give results in closer agreement with the experimental data. Results in Fig. 18 show that *k-ε* model with compressibility correction performs relatively well in capturing the mixing layer and the length of the potential core.

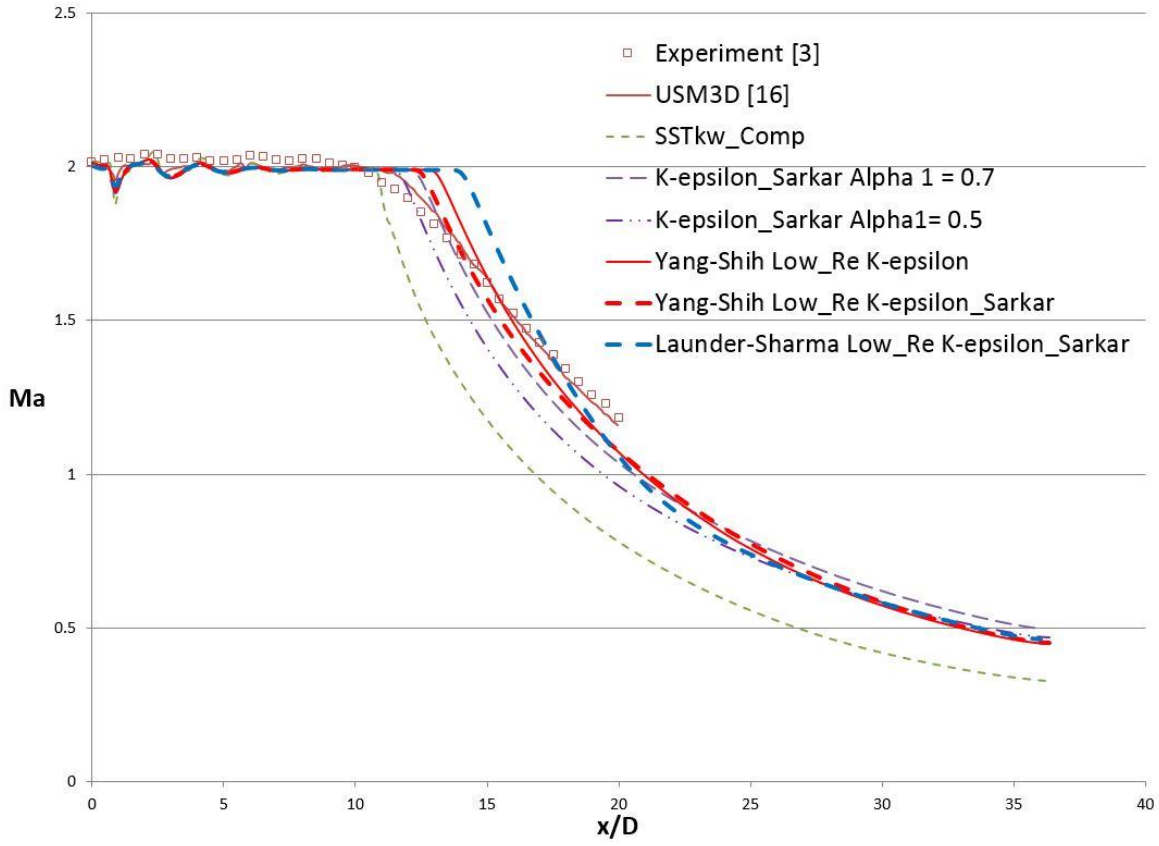

Figure 18 Variation in Mach number along the centerline from the jet exit for Seiner nozzle using various standard turbulence models with Sarkar's compressibility correction.

The importance of capturing the near wall boundary layer profile has been highlighted in the literature by the results of low Reynolds number *k*-*ε* model. Figure 18 shows that the low Reynolds number *k*-*ε* model compressibility correction performs almost as well as the standard *k*-*ε* model with compressibility correction. To evaluate the effect of changing the coefficient of the dilation dissipation term α_1 in compressibility correction, values of $\alpha_1 = 0.5$, 0.7, and 1.5 were tested against the reference value of 1.0 in the standard *k*-*ε* model. Results are presented in Fig. 19. As α_1 is increased, the length of the potential core also increases. This is expected since the effect of compressibility correction increases with increase in the value of α_1. Results in Fig. 19 show that the model with α_1 of 0.5 captures the mixing layer and length of the potential core better than the model with other values of the coefficient. However, even the best result using the standard *k*-*ε* model with compressibility correction fails to capture the experimental results and the USM3D results [16].

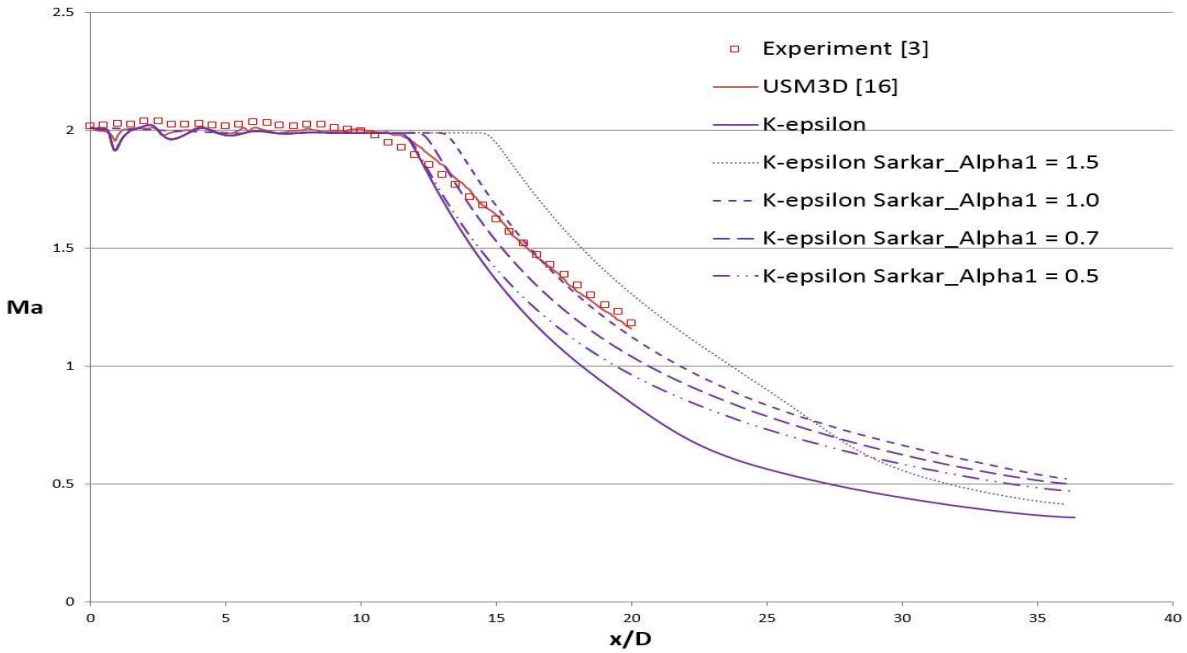

Figure 19 Variation in Mach number along the centerline from the jet exit for Seiner nozzle using *k*- *ε* model with various values of α_1 in Sarkar's compressibility correction.

The results from using the low Reynolds number k-ε models of Yang-Shih, Abid, and Launder-Sharma with compressibility correction are shown in Fig. 20. This Figure shows that the compressibility corrected models surprisingly deviate from the experimental data or do not show any significant improvement. The models with compressibility correction predict either a longer or same potential core length, and nearly the same mixing layer velocity decay rate. It has been noted by Gross et al. [17] that Sarkar's compressibility correction underpredicts the skin friction by 18 % at Mach 4. From Fig. 13, it can be seen that the SST k-ω baseline model captures the length of potential core quite accurately compared to the experimental data. The fact that SST k-ω performs the best in capturing the length of the potential core agrees with the conventional knowledge that SST k-ω model predicts the wall boundary layer character accurately for wide range of Mach numbers and geometries. Figure 21 compares the skin friction data employing the Abid's low Reynolds number k-ε model with and without compressibility correction, SST k-ω model, and k-ε model with and without compressibility correction. These models are chosen for comparison since they capture the length of the potential core quite well. Figure 21 shows that Abid's low Reynolds number k-ε model with compressibility correction overpredicts the skin friction compared to the model without compressibility correction. However, this phenomena is prevented for the standard k-ε model since it uses a wall function to calculate the skin friction coefficient. The skin friction coefficient calculated by the k-ε model matches well with that of SST k-ω model while the skin friction coefficient calculated from Abid's low Reynold number k-ε model fails to match that from the SST k-ω model. This results indicates that the standard k-ε model does not perform well because it requires wall function while the low Reynolds number k-ε models do not perform well since the compressibility

correction makes the models overpredict the skin friction coefficient resulting in longer potential core.

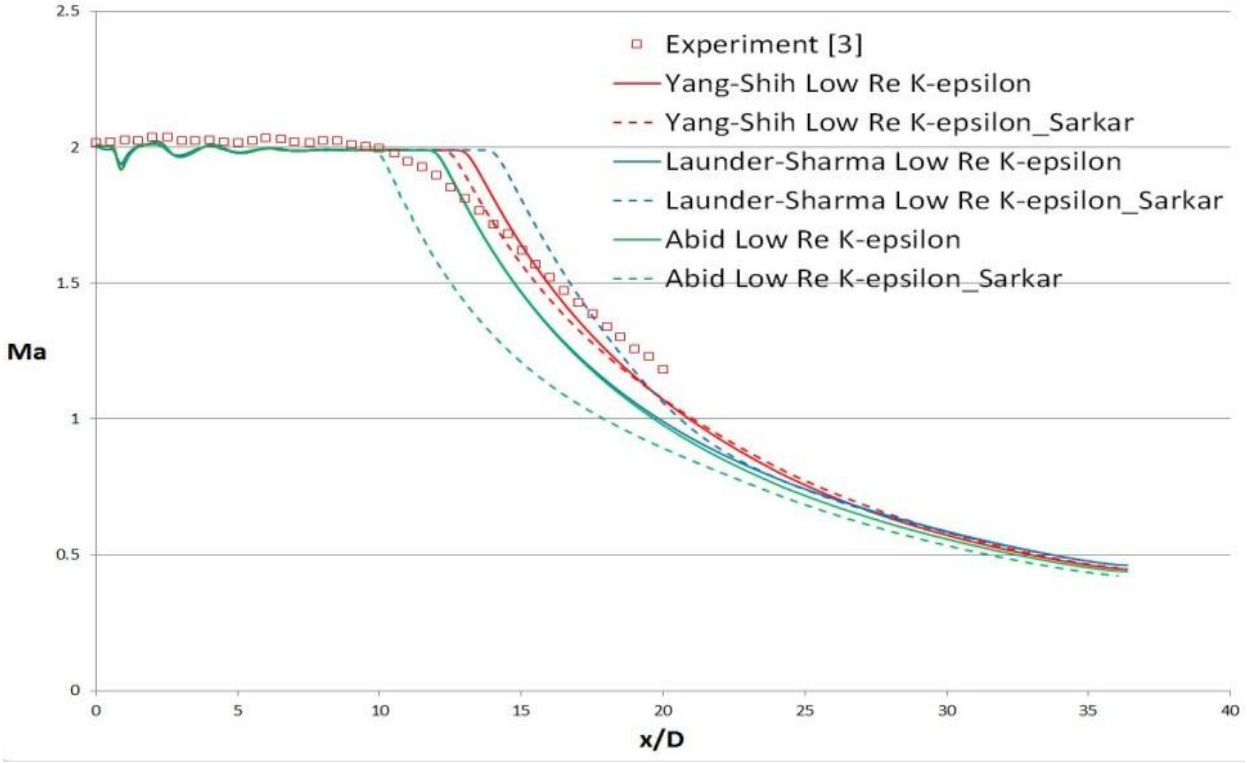

Figure 20 Variation in Mach number along the centerline from the jet exit for Seiner nozzle using different low Reynolds number *k*- *ε* models with and without Sarkar's compressibility correction.

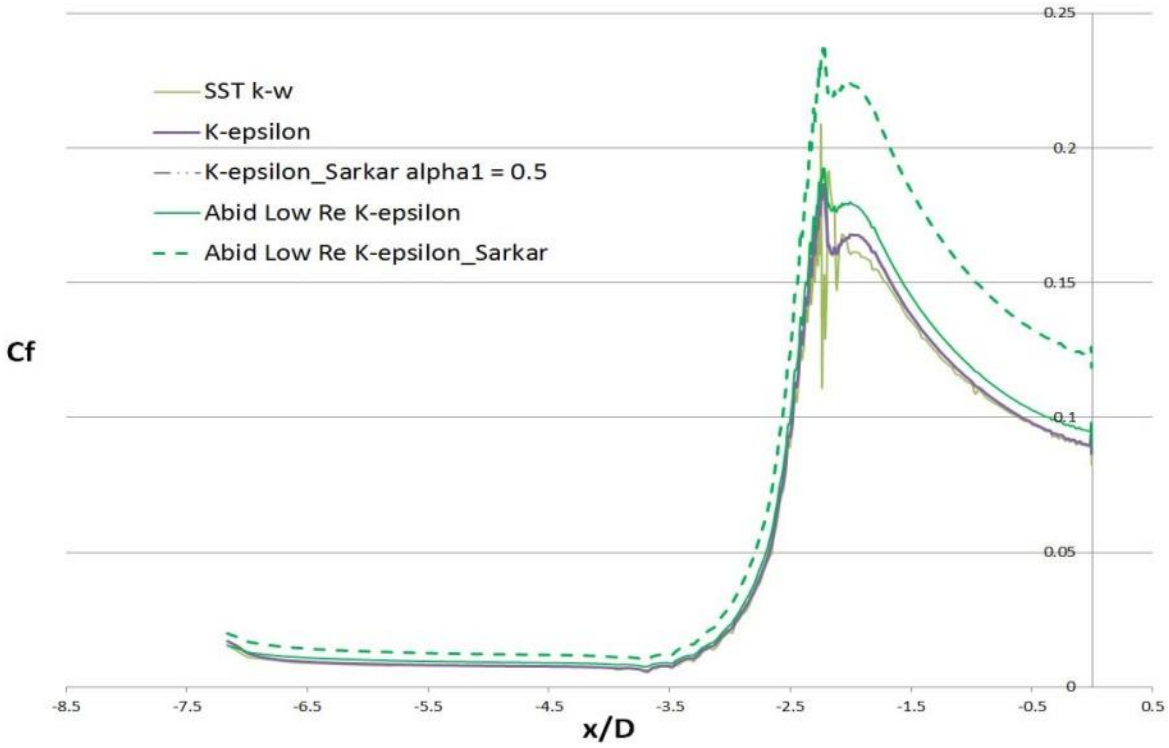

Figure 21 Comparison of Skin Friction coefficient on the wall of Seiner nozzle using various versions of *k- ε* models with and without Sarkar's compressibility correction; x = 0 is the jet exit.

SST *k-ω* model with compressibility correction has been previously used to simulate the jet exhaust from Eggers nozzle which also shows significantly thicker shear layer due to a large velocity difference between the freestream and the jet exhaust [18]. The model has been shown to accurately capture the mixing layer and the length of the potential core using the USM3D flow solver [18]. SST *k-ω* model without the Sarkar's compressibility correction and with the compressibility correction embedded in Fluent was also employed. However, as shown in Figs. 13 and 18, the Fluent simulation using SST *k-ω* model with and without compressibility correction fails to agree with the experimental data and USM3D results. The difference between the flow solver USM3D and ANSYS Fluent is that USM3D code uses a method proposed by Suzen and Hoffman [15] where the Sarkar's compressibility correction is only applied in the free shear layer and is turned-off near the wall. SST *k-ω* model with compressibility correction embedded in Fluent also turns the correction on and off depending on the distance to the wall.

However, the correction term in Fluent does not include pressure dilation and dilation dissipation which are included in Sarkar's correction. Similar effect can be achieved with a wall function utilized by the standard k-ε model since the method proposed by Suzen and Hoffman [15] also completely turns-off the compressibility correction in the near wall region. However, there is inherent difference in the use of wall function vs. the calculation of transport equation down to the wall. It can be concluded that a blending function applied to the compressibility correction only in the shear flow region may be needed to correctly capture the mixing layer growth and the length of the potential core.

5.3.3 Results with Compressibility Correction for Wray-Agarwal Model

The method to obtain the compressibility correction for Wray-Agarwal model was described in Section 3.3. To compare the effects of two compressibility corrections, that of Sarkar and Wilcox, they are tested against each other. However, application of different forms of the compressibility correction is not limited to these two because the type of compressibility correction can easily be switched as suggested in Eq. (53). Moreover, different coefficients in the compressibility correction are tested to closely match the experimental results. The major difference between the compressibility correction of Sarkar and Wilcox is the existence of a Heaviside function in Wilcox's formulation that turns off the compressibility term near the wall. As mentioned in the previous section, compressibility correction can have a negative effect on the boundary layer profile. In Fig. 22, Mach number profile is plotted against a normalized distance at the centerline for WA model with either the Wilcox correction or Sarkar correction. The compressibility coefficient, C_{comp}, is plotted with different values of 0.01, 0.05 and 0.3. It is evident from this figure that compressibility corrected WA model based on either Wilcox or Sarkar correction gives almost the same results. Also, C_{comp} of 0.05 in WA model matches the

SST *k-ω* results with compressibility correction the best. However, like SST *k-ω* and *k-ε* models with compressibility correction, WA model does not perfectly capture the experimental results along the centerline.

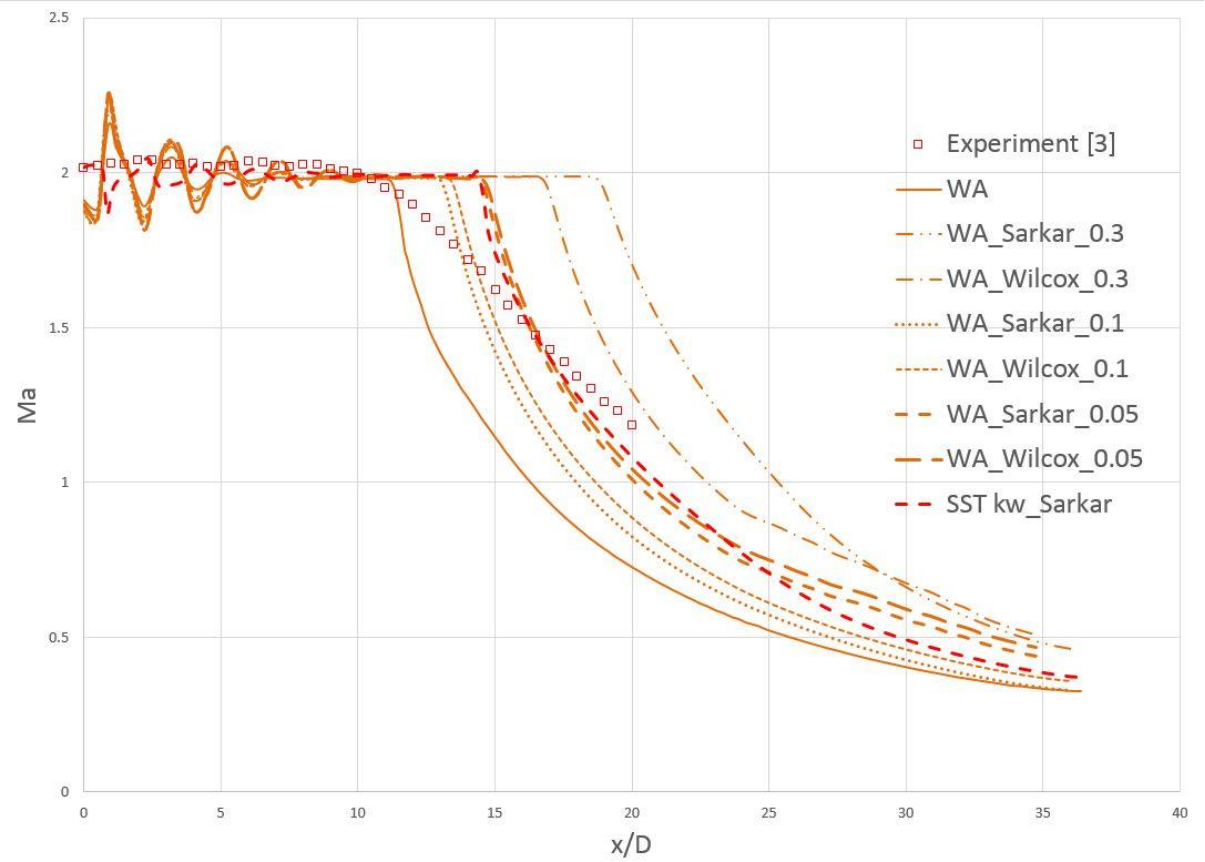

Figure 22 Variation in Mach number along the centerline from the jet exit for Seiner nozzle using Wray-Agarwal model with Sarkar's compressibility correction.

5.4 Eggers Nozzle Results

Eggers nozzle is another case with shear layer similar to that in case of Seiner nozzle results. This case provides experimental data in radial direction at various horizontal locations along the x-axis that allows for a more detailed and better comparison of results from various turbulence models. Simulations for Eggers nozzle were conducted with SA model, SST *k-ω* model with and without compressibility correction, the standard *k-ε* model with and without compressibility correction, Launder and Sharma low Reynold number *k-ε* models with and

without compressibility correction and the Wray-Agarwal model with and without compressibility correction.

5.4.1 Results without Compressibility Correction

Results from baseline turbulence models without compressibility correction in Fig. 23 show the normalized velocity at the centerline of the nozzle obtained from *k-ε*, Launder-Sharma Low Reynolds *k-ε,* Yang-Shih Low Reynolds *k-ε*, SST *k-ω*, and Wray –Agarwal turbulence models without compressibility correction. Results indicate that all models except for SST *k- ω* fail to capture the length of potential core. However, *k- ε* variant models including both the Low Reynolds k-ε models capture the centerline profile very well downstream. A good performance of low Reynolds *k-ε* models is also expected since they performed very well in the case of Seiner nozzle. Figure 24 shows the radial velocity profile at the exit of the nozzle. The results from Fig. 24 show that the velocity profiles from different models are very similar to each other at the exit of the nozzle. It confirms the expectation that there will not be much difference in velocity profiles at the exit.

It is worthy to pay attention to Figures 25, 26 and 27. Figure 25 shows the radial velocity profile at x/r_{exit} = 26.93. Figure 26 shows the radial velocity profile at x/r_{exit} = 51.96. Figure 27 shows the radial velocity profile at x/r_{exit}=121.3. All figures indicate that, although Wray-Agarwal turbulence model like other models fails to capture the exhaust plume characteristic along the centerline, it captures the radial velocity profiles very well. Figures 23 and 25 show that the results from Wray-Agarwal turbulence model are slightly higher than the experimental value along the axis. However, away from the centerline, the velocity profiles quickly capture the experimental results. The next best baseline model that captures the experimental results well is the Launder-Sharma Low Reynolds *k-ε* model. Although Launder-Sharma Low Reynolds *k- ε*

model performs better in capturing the experimental radial velocity profile at x/r_{exit} = 51.96 in Fig. 26, Wray-Agarwal again outperforms in capturing experimental radial velocity profile at x/r_{exit} =121.3 as shown in Fig. 27. SST *k-ω* and SA turbulence models without compressibility correction fail to capture the experimental results.

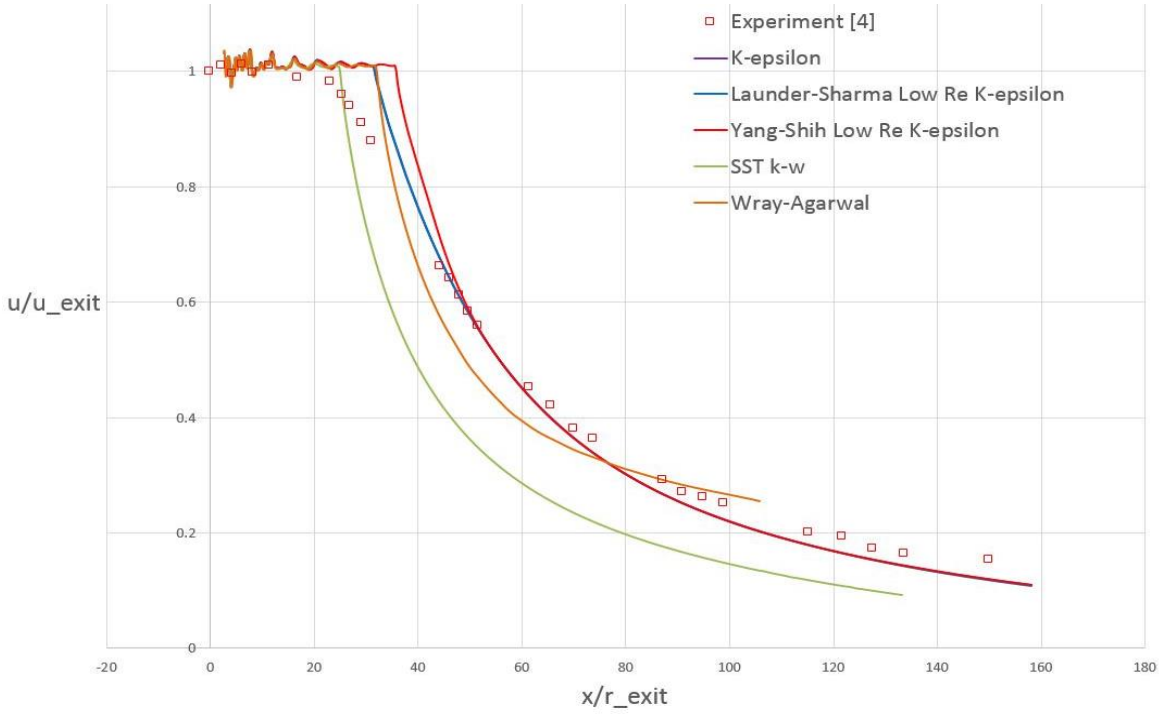

Figure 23 Variation in u/u_exit along the centerline from the jet exit for Eggers nozzle using various baseline turbulence models without compressibility correction.

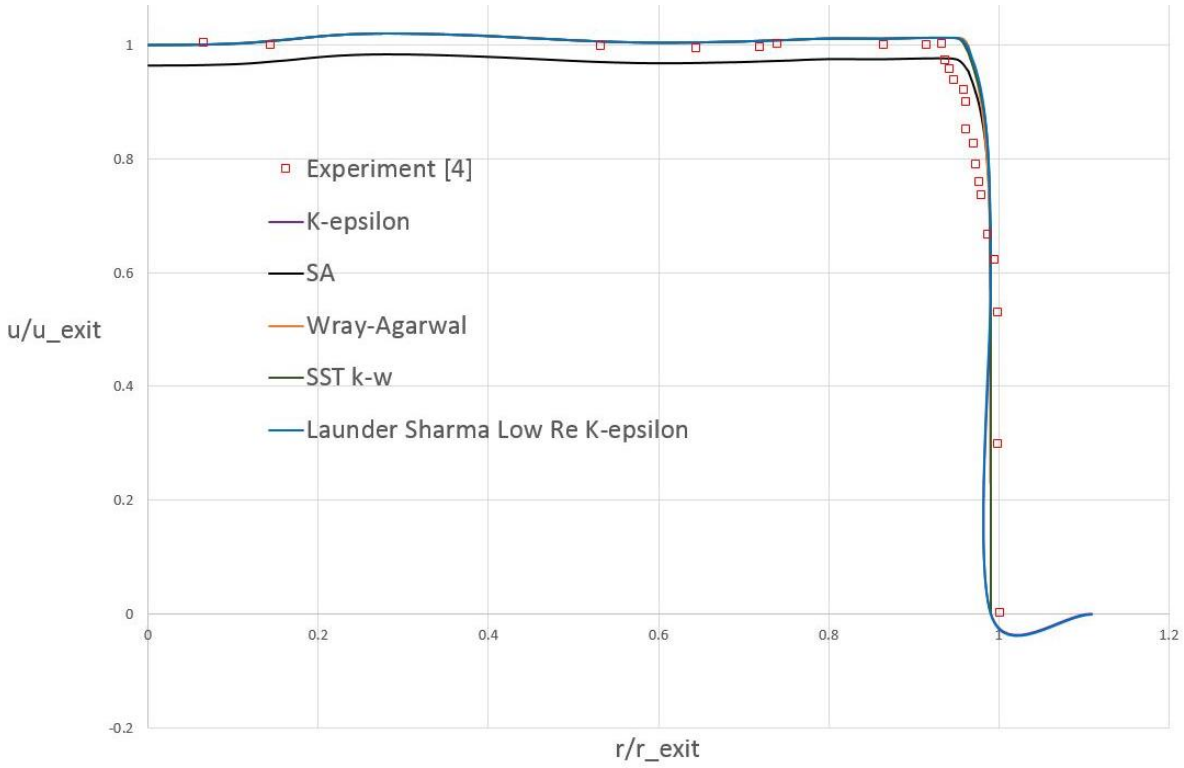

Figure 24 Variation in u/u_exit along the radial direction at x/r_exit=3.06 for Eggers nozzle using various baseline turbulence models without compressibility correction.

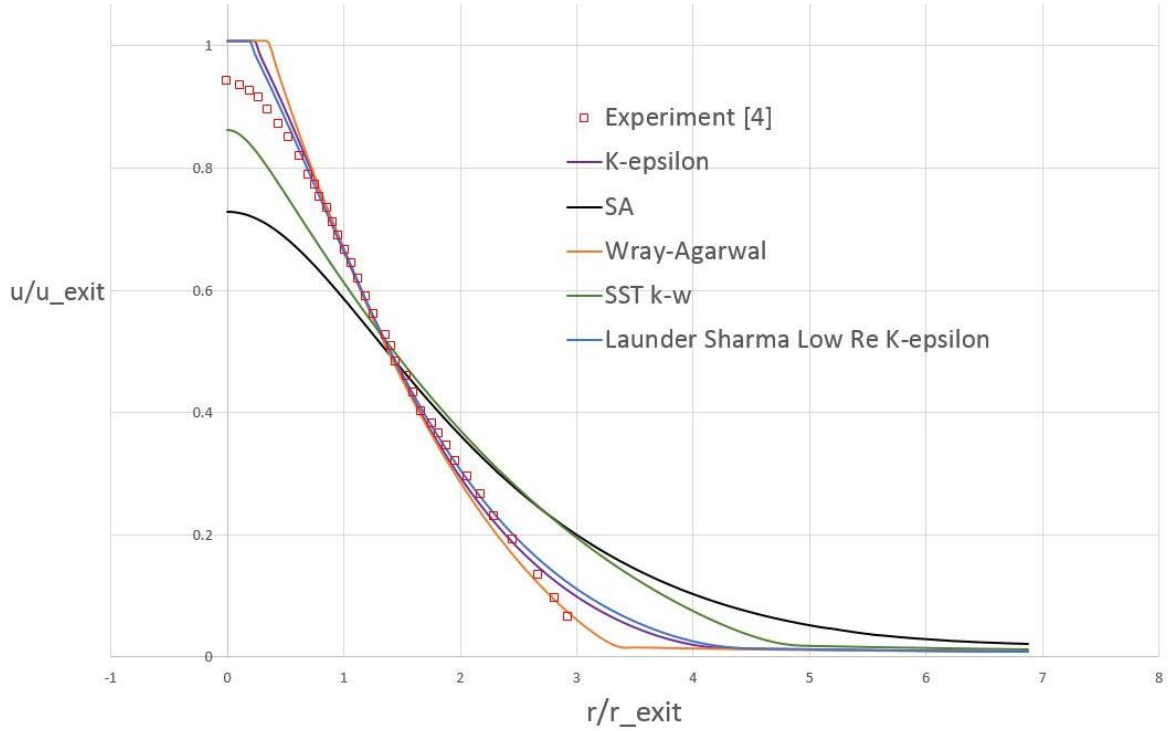

Figure 25 Variation in u/u_exit along the radial direction at x/r_exit=26.93 for Eggers nozzle using various baseline turbulence models without compressibility correction.

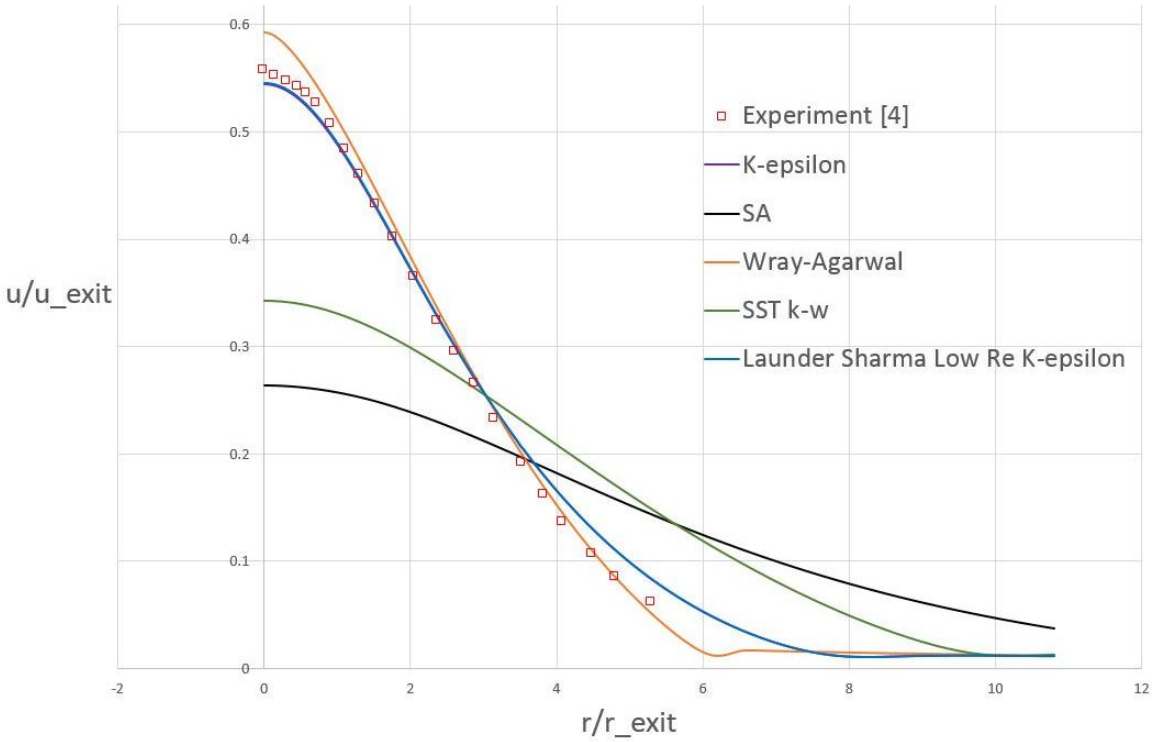

Figure 26 Variation in u/u_exit along the radial direction at x/r_exit=51.96 for Eggers nozzle using various baseline turbulence models without compressibility correction.

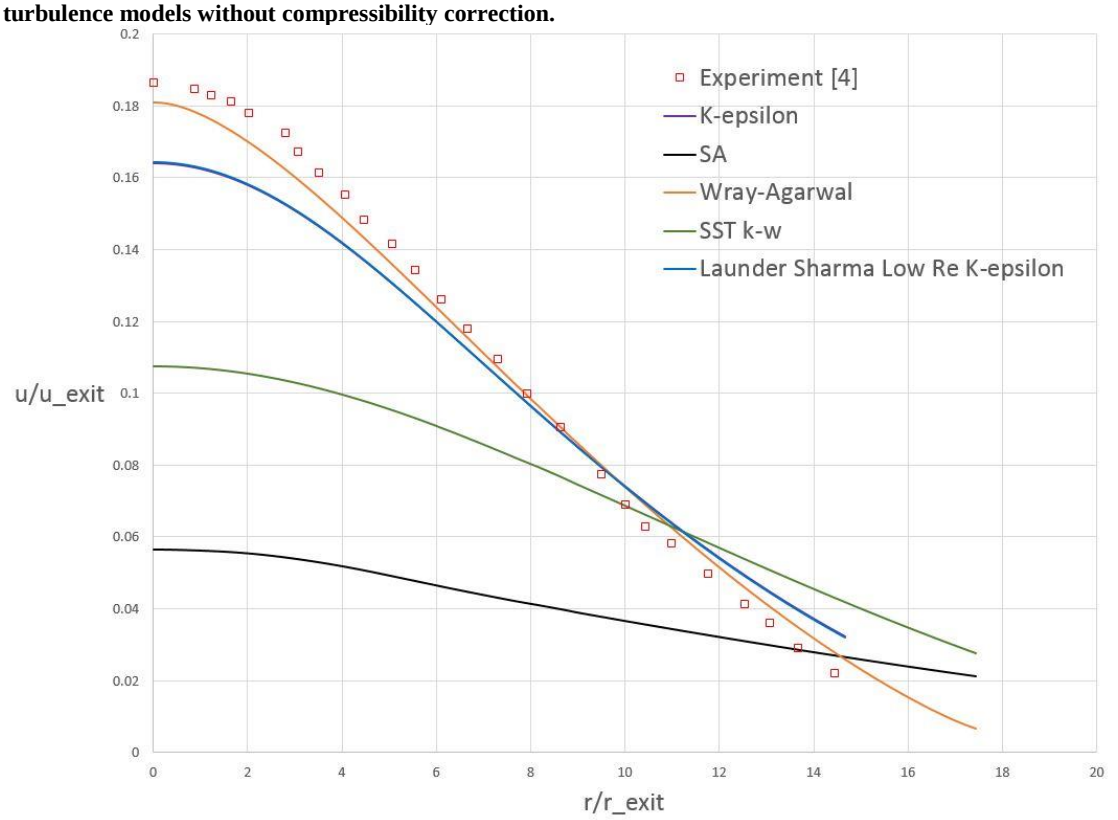

Figure 27 Variation in u/u_exit along the radial direction at x/r_exit=121.3 for Eggers nozzle using various baseline turbulence models without compressibility correction.

5.4.2 Results with Compressibility Correction SST *k-ω, k-ε* and Low Reynolds Number *k-ε* Models

In this section, the effects of compressibility correction for SST *k-ω, k-ε* and Low Reynold number *k-ε* are examined. All compressibility correction compared in this section use the Sarkar's compressibility coefficient of 0.1. As was mentioned in section 5.3.2, there are multiple variables that affect the results in case of thick shear layer. In particular, the need for compressibility correction and accurate prediction of boundary layer profile near the nozzle exit was highlighted. Also, the results for Seiner nozzle indicate that the compressibility correction has a negative effect on the boundary layer which results in the overall inaccuracy for turbulence models in prediction of supersonic jet exhaust. Therefore, while compressibility correction is needed in shear layer to accurately capture the plume characteristics, it should be carefully turned off to decrease the negative effect it has on the boundary layer near nozzle exit.

Like previous results for Seiner nozzle, low Reynolds number *k-ε* models with compressibility correction did not improve the accuracy of the result in predicting the length of potential core as shown in Fig. 28. Surprisingly the models with compressibility correction produced more inaccurate results in predicting the length of the potential core. However, the compressibility correction's beneficial effect in the prediction of the velocity profile can be demonstrated when comparing the radial velocity profile results and experimental data. As mentioned in section 5.4.1, the velocity profiles predicted from different turbulence models are very similar at the exit of the nozzle as shown in Figs 29 and 30. Fig 32 shows how SST *k-ω* model with Sarkar's compressibility correction improves the results remarkably in capturing the experimental results compared to the baseline model without compressibility correction. Figure 32 shows the radial velocity profile at $x/r_{exit} = 26.93$. In this figure, while SST *k-ω* model with

compressibility correction goes right through the experimental data profile, SST *k*-ω without the compressibility correction slightly underpredicts the data. Figures 34 and 36 show the radial velocity profile using the SST *k*-ω model with and without compressibility correction at x/r_{exit} = 51.96 and x/r_{exit} = 121.3, respectively. In these two figures, the difference between the performance of the compressibility corrected SST *k*-ω and the its baseline model becomes greater, showing the beneficial effect of the compressibility correction.

It is worth noting that the compressibility correction may have a negative effect in predicting the experimental data in some cases if the compressibility correction is not turned-off in the wall boundary layer near the nozzle exit. Figures 33 and 35 show the radial velocity profiles obtained using the *k*-ε and low Reynold number *k*-ε turbulence model at x/r_{exit} = 51. 96 and x/r_{exit} = 121.3, respectively. The velocity profiles obtained from these two models with compressibility correction actually deviate from the experimental data. This phenomena may be due to the fact that the compressibility correction has a negative effect in the prediction of boundary layer near the jet exit. The fact that these two models do not have the ability to turn-off the compressibility correction near the wall may cause the inaccuracy in prediction of the radial velocity profile. This argument is further supported by examining the Wray-Agarwal model results in Fig. 34 and 36. In these two figures, the Sarkar's compressibility correction which applies the correction to all the region including the boundary layer performs considerably worse than the Wilcox compressibility correction which turns off the correction near the wall via the Heaviside function.

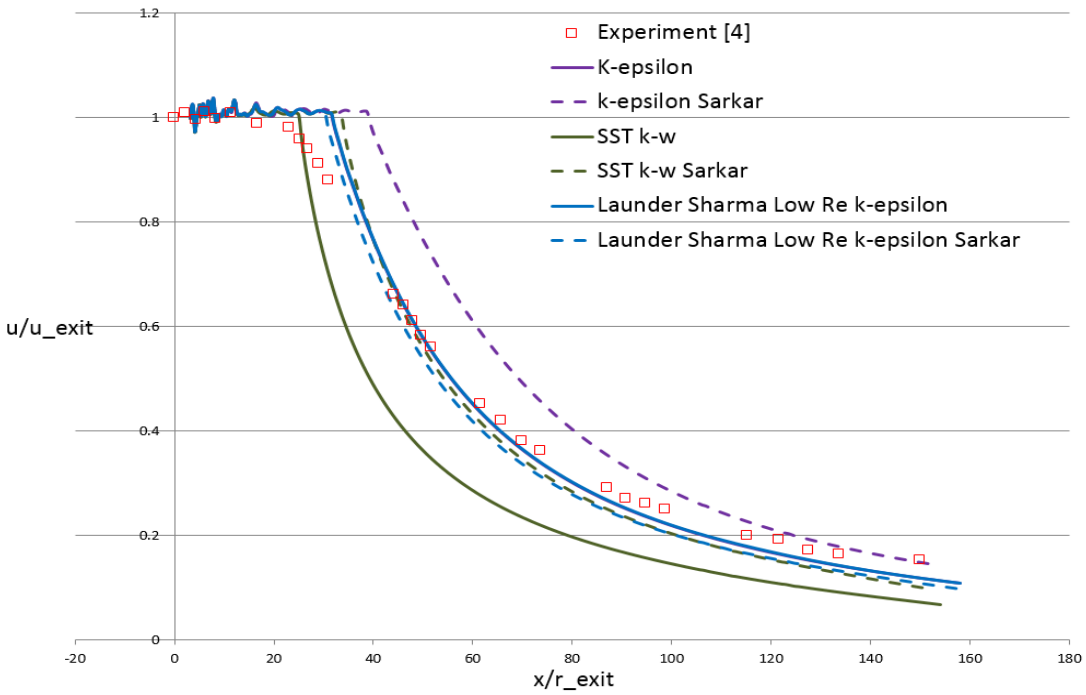

Figure 28 Variation in u/u_exit along the centerline from the jet exit for Eggers nozzle using various turbulence models with and without Sarkar's compressibility correction.

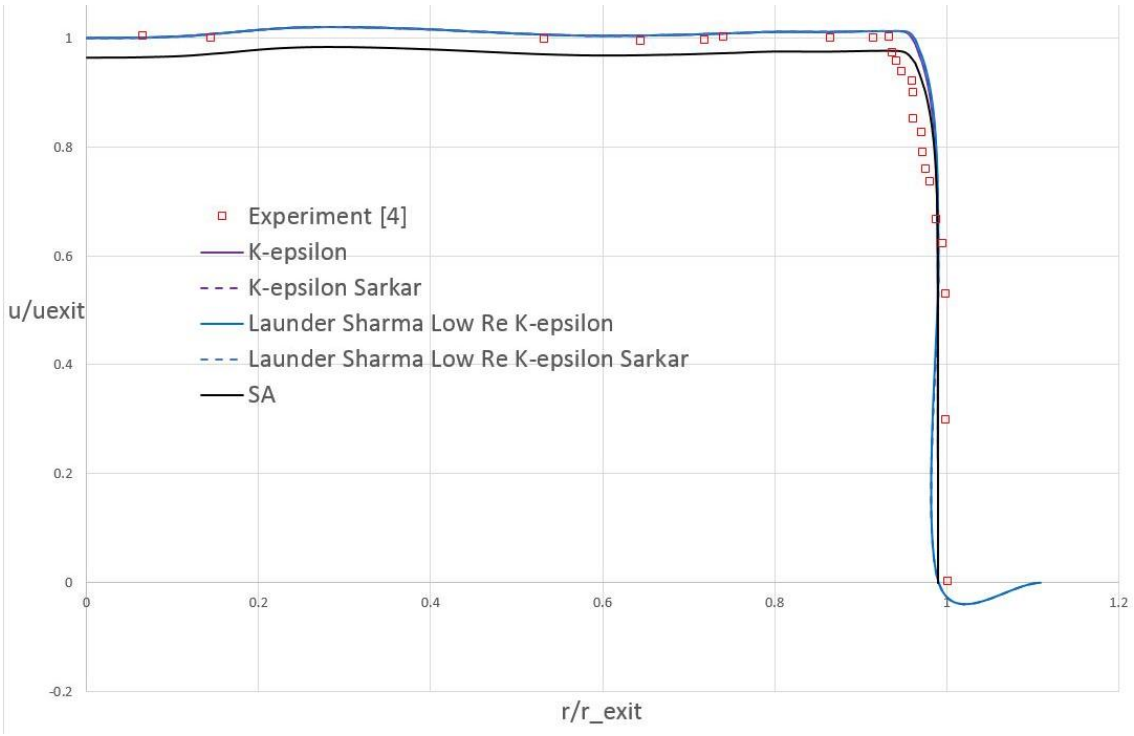

Figure 29 Variation in u/u_exit along the radial direction at x/r_exit=3.06 for Eggers nozzle using *k-ε*, low Reynold number *k-ε* turbulence model and SA models with and without Sarkar's compressibility correction.

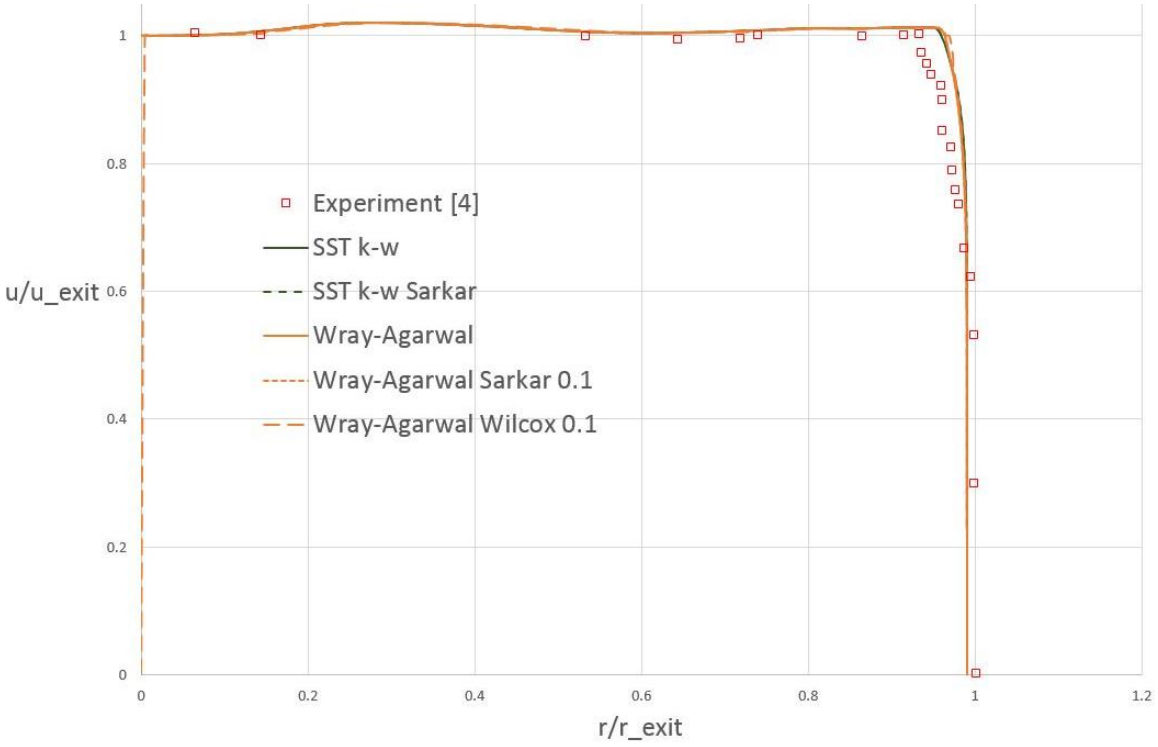

Figure 30 Variation in u/u_exit along the radial direction at x/r_exit=3.06 for Eggers nozzle using SST *k-ω* and Wray-Agarwal turbulence models with and without compressibility correction.

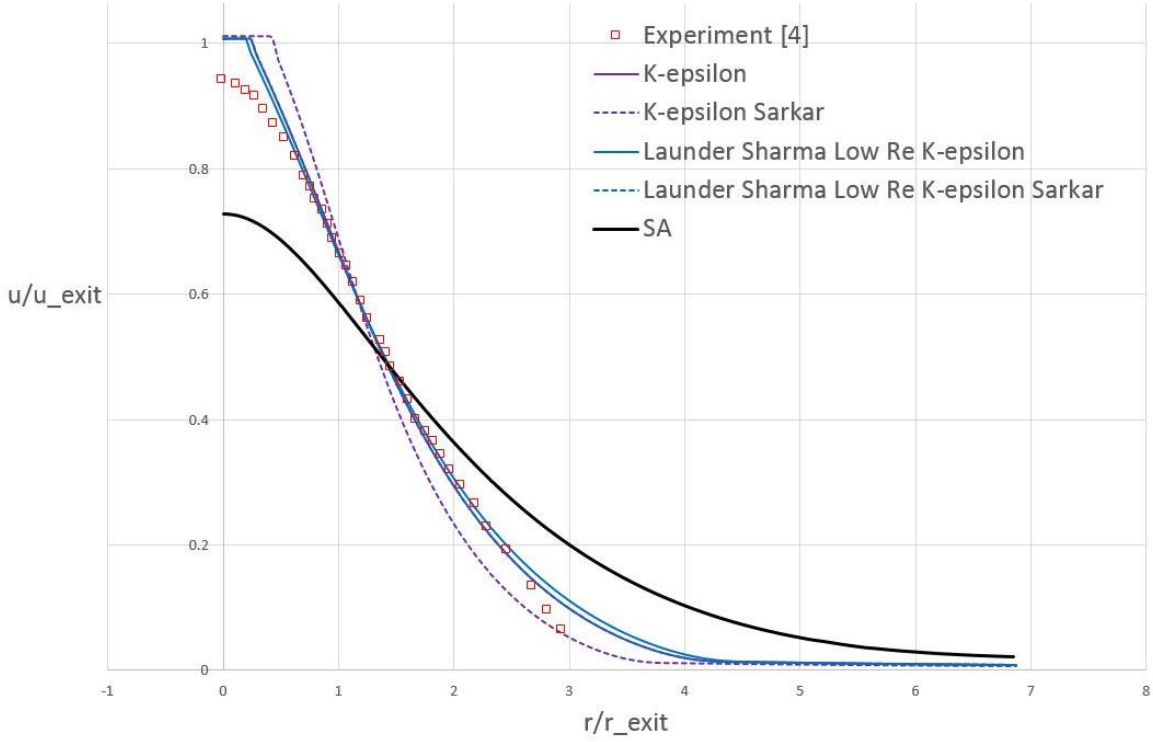

Figure 31 Variation in u/u_exit along the radial direction at x/r_exit=26.93 for Eggers nozzle using *k-ε*, low Reynold number *k-ε* turbulence model and SA models with and without Sarkar's compressibility correction.

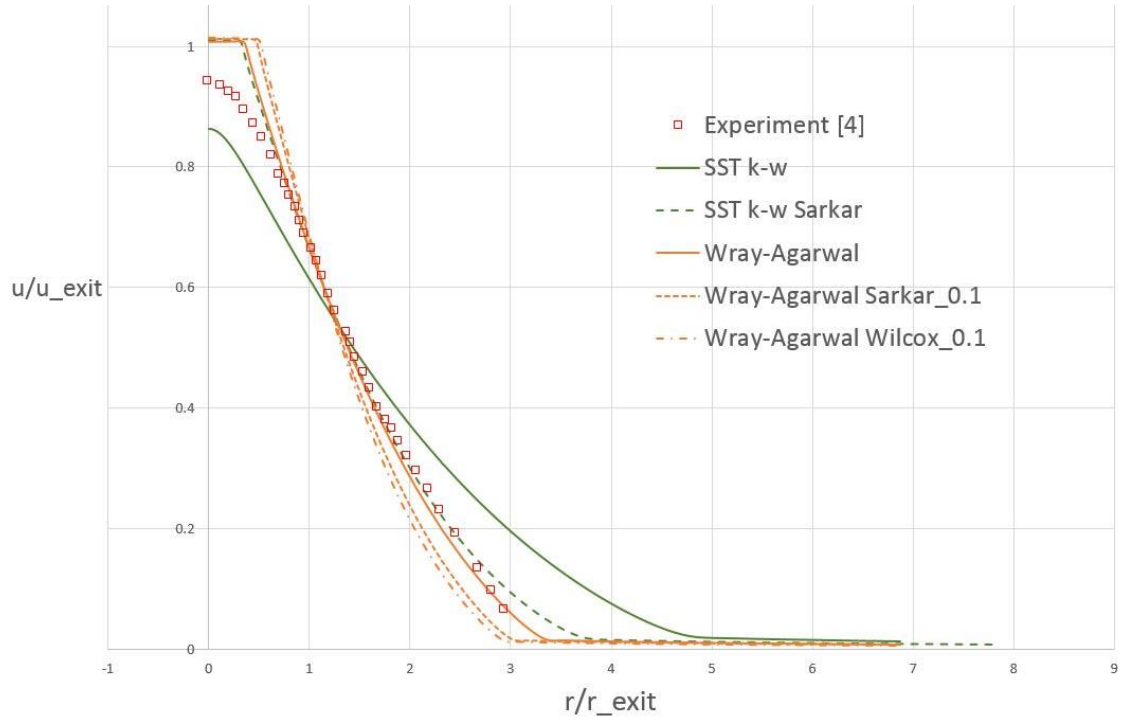

Figure 32 Variation in u/u_exit along the radial direction at x/r_exit=26.93 for Eggers nozzle using SST *k-ω* and Wray-Agarwal turbulence models with and without compressibility correction.

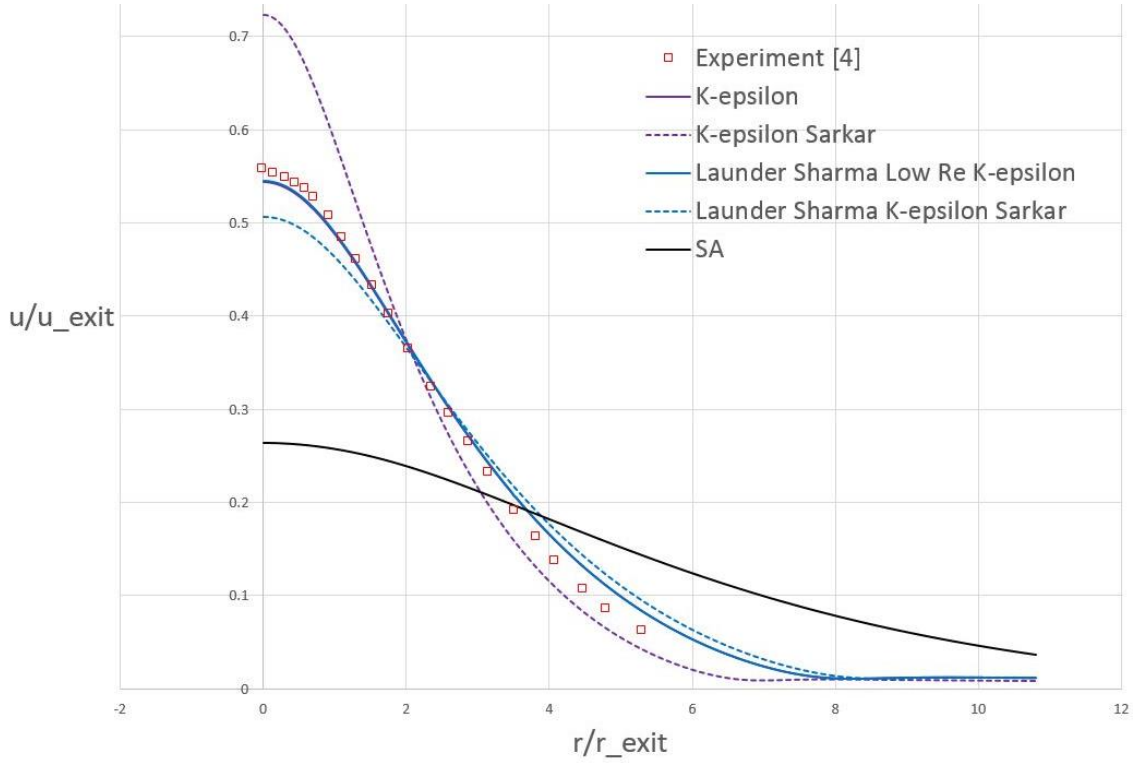

Figure 33 Variation in u/u_exit along the radial direction at x/r_exit=51.96 for Eggers nozzle using *k-ε*, low Reynold number *k-ε* turbulence model and SA models with and without Sarkar's compressibility correction.

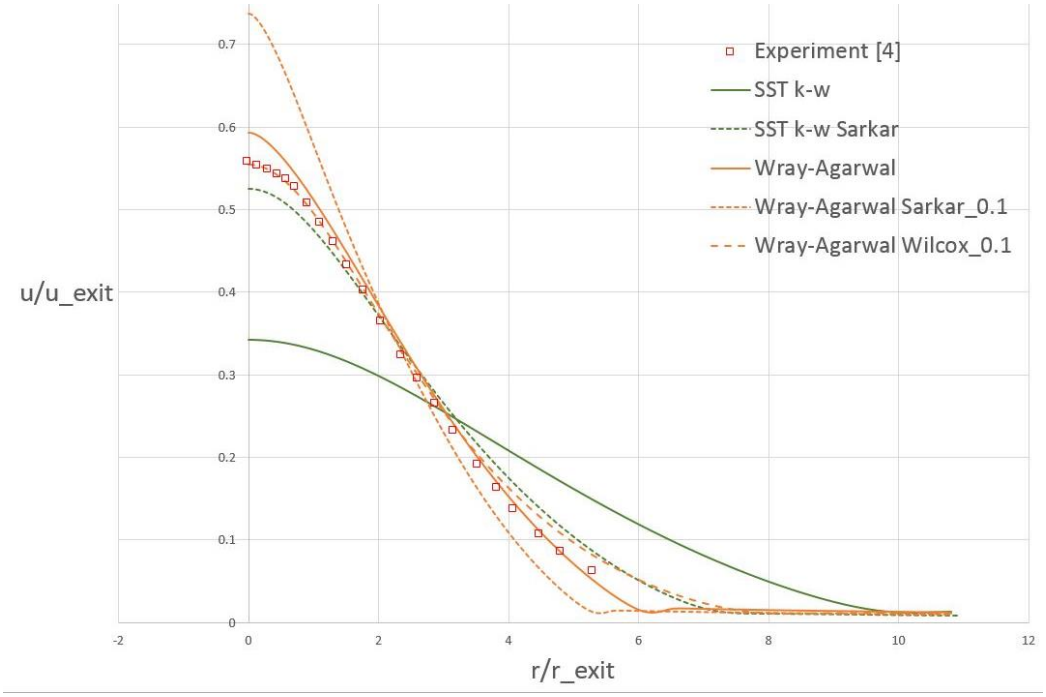

Figure 34 Variation in u/u_exit along the radial direction at x/r_exit=51.96 for Eggers nozzle using SST *k-ω* and Wray-Agarwal turbulence models with and without compressibility correction.

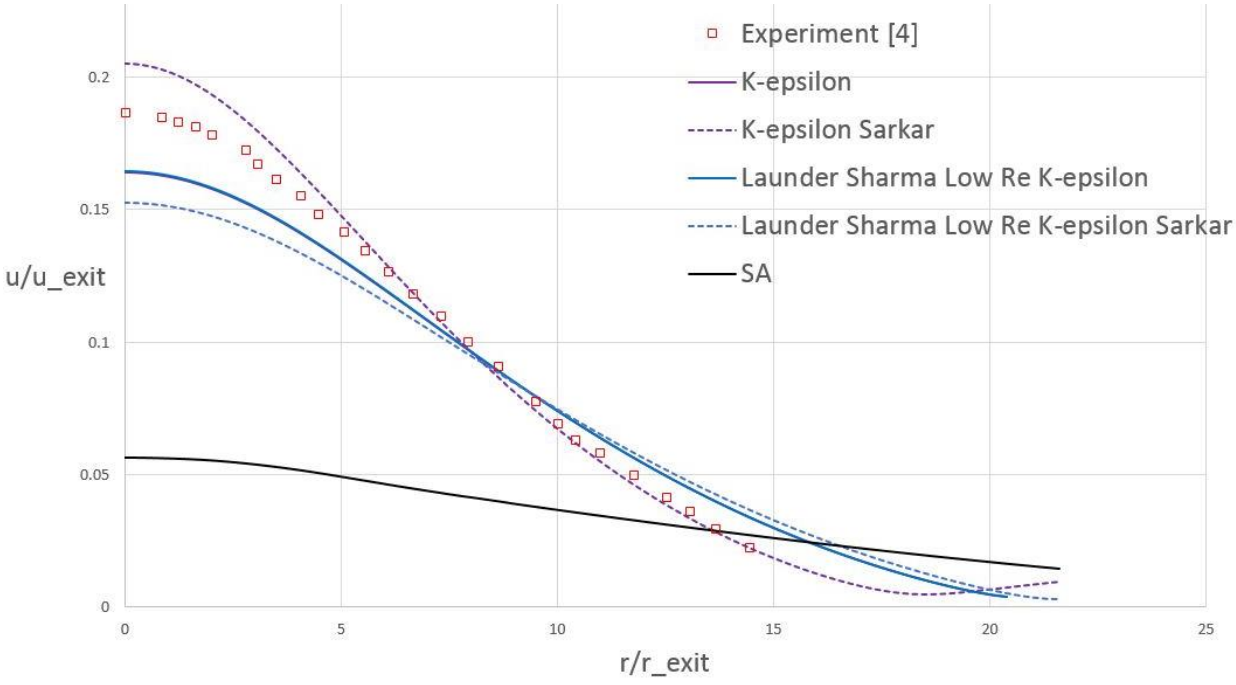

Figure 35 Variation in u/u_exit along the radial direction at x/r_exit=121.3 for Eggers nozzle using *k-ε*, low Reynold number *k-ε* turbulence model and SA models with and without Sarkar compressibility correction.

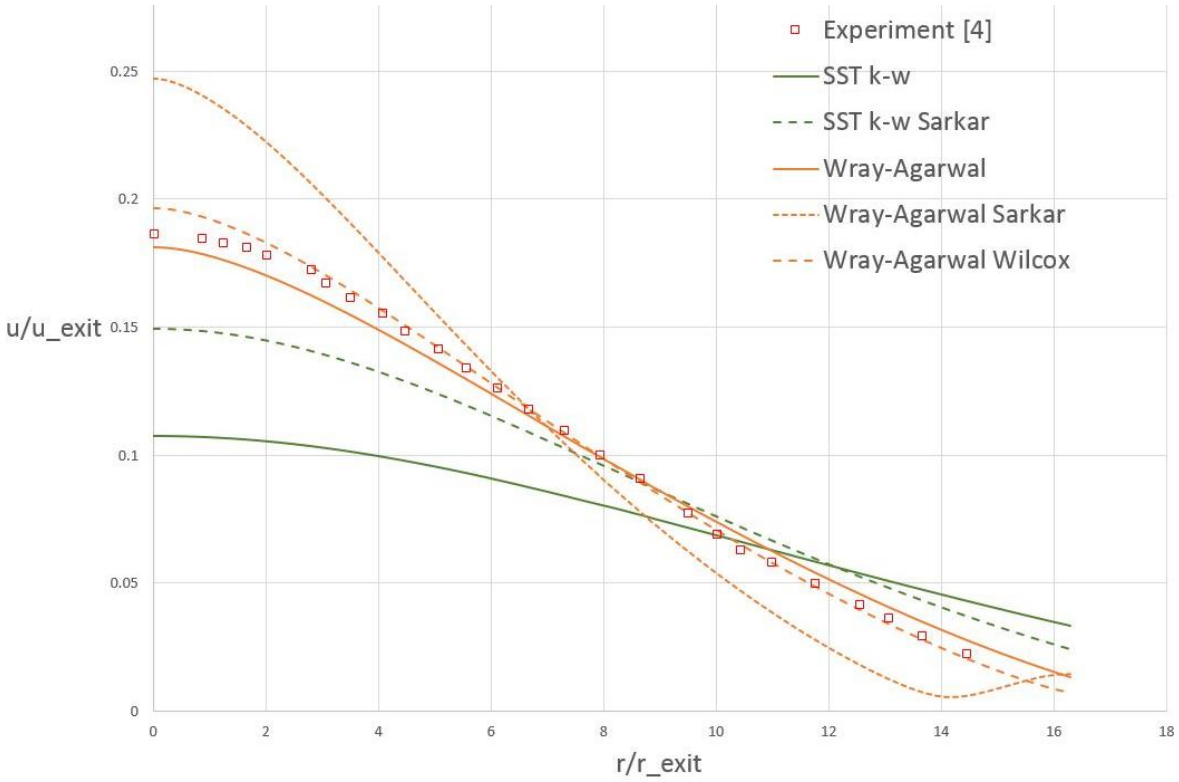

Figure 36 Variation in u/u_exit along the radial direction at x/r_exit=121.3 for Eggers nozzle using SST *k-ω* and Wray-Agarwal turbulence models with and without compressibility correction.

5.4.3 Results with Compressibility Correction for WA Model

In this section, the effects of compressibility correction for Wray-Agarwal turbulence model with two compressibility corrections are compared along with the SST *k-ω* model with compressibility correction. The form of compressibility correction is switched between that by Sarkar and that by Wilcox. The results from Wray-Agarwal model with and without compressibility correction suggest correction that Wray-Agarwal turbulence model with Wilcox compressibility correction performs the best.

Figure 36 shows the normalized velocity profile along the centerline. It shows that none of the models correctly captures the length of the potential core. However, the best agreement is obtained either from the Wray Agarwal model without compressibility correction or from Wray-Agarwal with Wilcox compressibility correction. Figures 38, 39 and 40, which show the radial

velocity profiles at x/r_{exit} = 26.93, x/r_{exit} =51.96 and, x/r_{exit} =1212.3, respectively, demonstrate that the Wray-Agarwal turbulence model with Wilcox compressibility correction formation captures the experimental results very well. WA model performs better in capturing the radial velocity profile than the SST *k-w* model with Sarkar's compressibility correction as can be seen in Figs. 32, 34, and 36. As mentioned in section 5.4.2, Sarkar's compressibility correction does not inhibit the presence of the correction near the nozzle wall which may be the cause of inaccuracy in the simulation.

An interesting observation from the results in that the Wray-Agarwal model without the compressibility correction always outperforms the results from the WA model with the compressibility correction. In Fig 38, it can be seen that the velocity profile from Wray-Agarwal model starts off slightly higher than the experimental data but quickly captures the experimental data and performs better than all other models from Fig. 40. It can be seen that the WA model without the compressibility correction performs as accurately as the model with Wilcox compressibility correction.

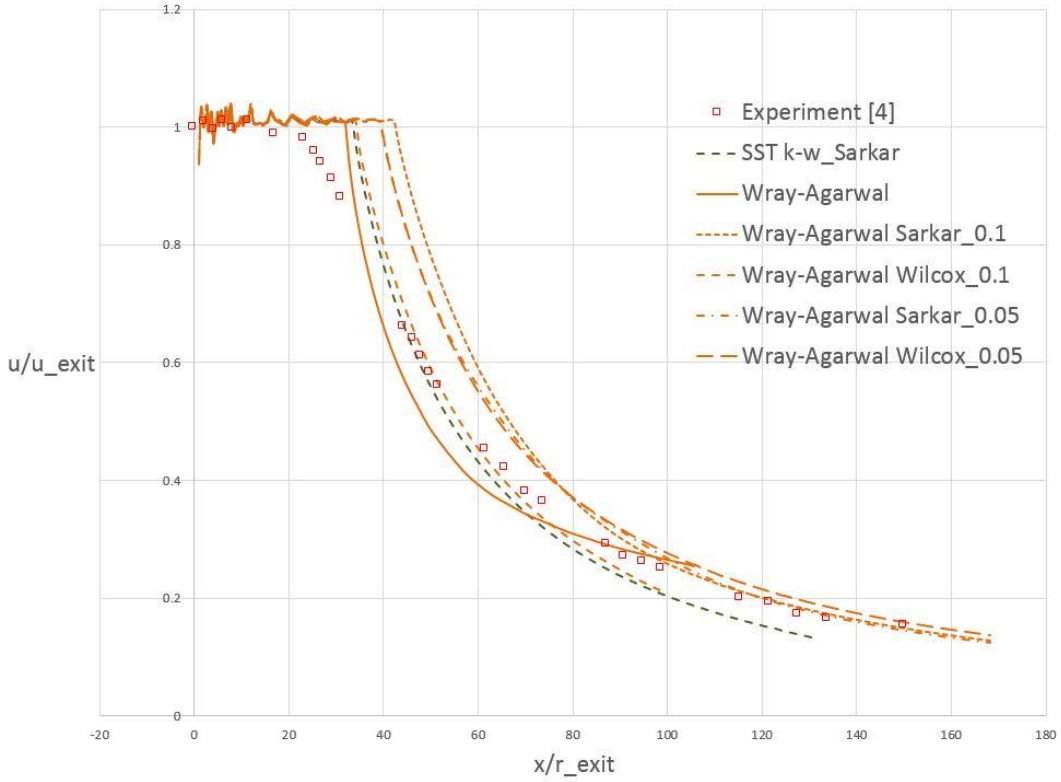

Figure 37 Variation in u/u_exit along the centerline from the jet exit for Eggers nozzle using Wray-Agarwal turbulence models with two different compressibility corrections.

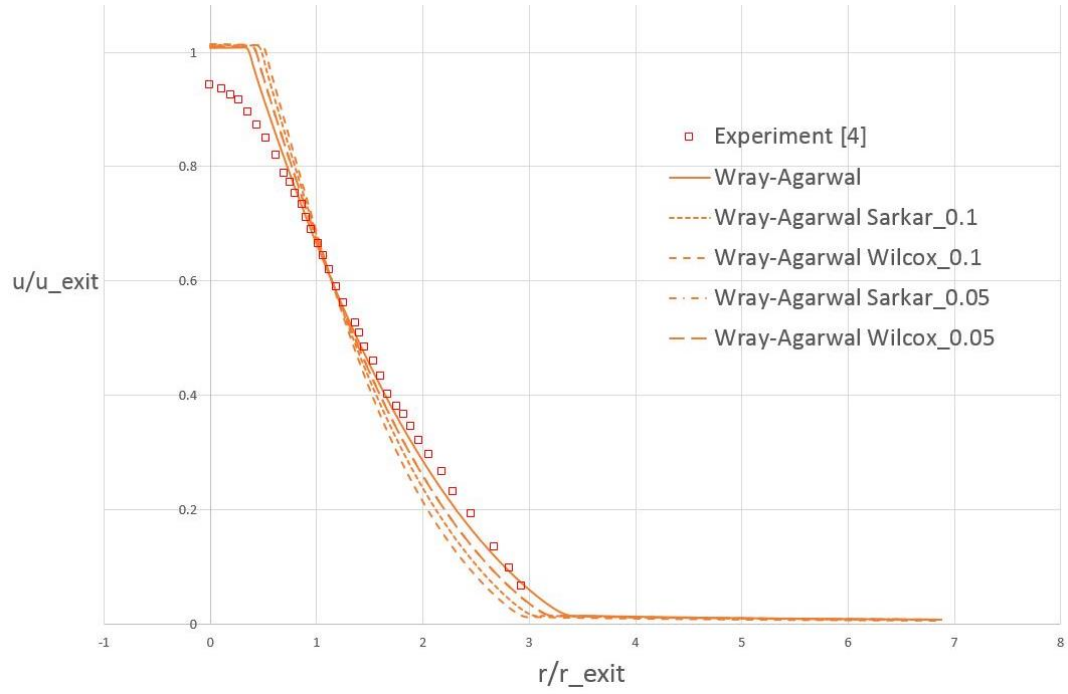

Figure 38 Variation in u/u_exit along the radial direction at x/r_exit=26.93 for Eggers nozzle using Wray-Agarwal turbulence models with two different compressibility corrections.

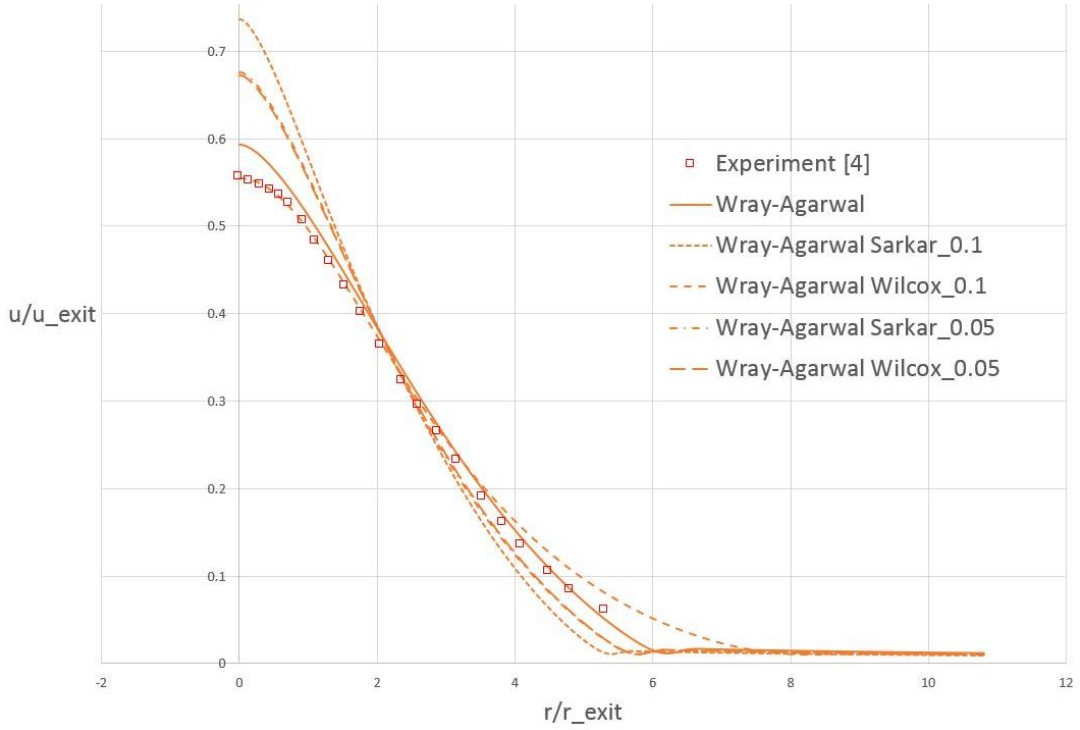

Figure 39 Variation in u/u_exit along the radial direction at x/r_exit=51.96 for Eggers nozzle using Wray-Agarwal turbulence models with two different compressibility corrections.

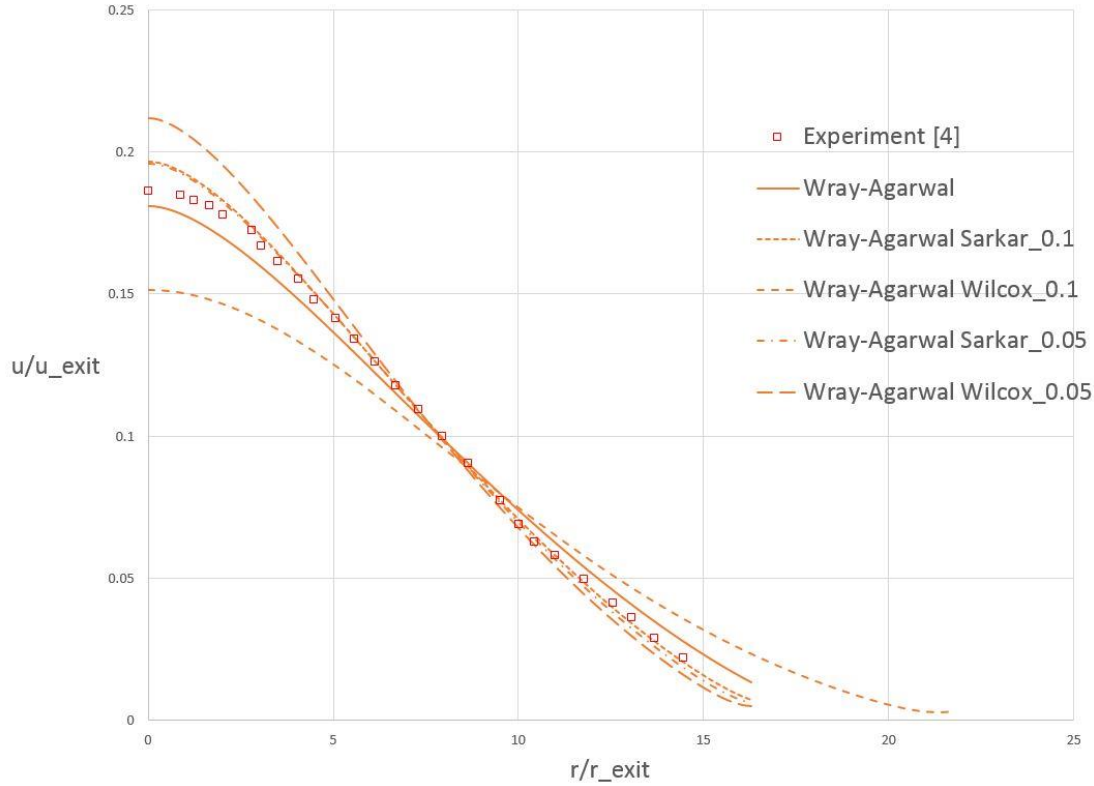

Figure 40 Variation in u/u_exit along the radial direction at x/r_exit=121.3 for Eggers nozzle using Wray-Agarwal turbulence models with two different compressibility corrections.

Chapter 6
Conclusions

In this thesis, three benchmark axisymmetric supersonic exhaust jet flows have been computed using ANSYS Fluent with a number of eddy viscosity turbulence models. Four baseline eddy-viscosity turbulence models (SA, SST k-ω, standard k-ϵ and WA) and their compressibility corrected forms, and the low Reynold number k-ε models by Yang-Shih, Abid, Launder-Sharma with Sarkar compressibility correction were employed in the computations. An auto adapted mesh was used to refine the grid in areas of large density gradients. For the Putnam nozzle, all baseline turbulence models were able to correctly predict the jet shear layer and the shock structures in the plume. The inclusion of Sarkar's compressibility correction in the turbulence models did not show further improvement in the results. A thicker shear layer exists in exhaust jet from Seiner nozzle. In this case, the baseline turbulence models were not able to correctly capture the growth of shear layer and the length of the potential core of the jet. The inclusion of compressibility corrections improved results somewhat but still satisfactory results could not be obtained. The good performance of low Reynolds k-ε models indicates that accurate prediction of boundary layer profile at jet exit is needed in the prediction of shear layer mixing rate and potential core length. It was shown that the compressibility correction may have a negative effect on simulation of boundary layer by computing the skin friction on the nozzle wall using various models. Finally, it was shown for Eggers nozzle that the models that do not have the ability to turn-off the compressibility correction in boundary layer performed worse than their baseline models without compressibility correction in several cases. Combined with the knowledge that the compressibility correction may have a negative effect on the boundary layer profile accuracy, the computation for two case reconfirmed that capturing boundary layer profile

at the nozzle exit is important in capturing the shear layer mixing rate and the length of the potential core.

Another highlight of the thesis is the performance of the WA model. Although it did not capture the Mach number profile in Seiner nozzle quite well, it performed very well for Eggers nozzle. In evaluation of the results with WA model, it was found that the WA model with Wilcox compressibility correction performed the best in capturing the velocity profile in shear layer. However, all of the models were not able to capture the length of the potential core even for the Eggers nozzle.

This study shows the importance of compressibility corrections in the accurate prediction of compressible mixing layers and jet core length. However, improvements are needed in turbulence modeling of compressible shear layer flows for accurate predictions of this class of flow fields.

Chapter 7
References

[1]"1st AIAA Sonic Boom Prediction Workshop." http://lbpw.larc.nasa.gov/ [retrieved October 2015]

[2] Putnam, L. E. and Capone, F. J., "Experimental Determination of Equivalent Solid Bodies to Represent Jets Exhausting into a Mach 2.20 External Stream," NASA-TN-D-5553, Dec. 1969.

[3] Seiner, J. M., Dash, S. M., and Wolf, D. E., "Analysis of Turbulent Underexpanded Jets, Part II: Shock Noise Features Using SCIPVIS," AIAA Journal, Vol. 23, No. 5, May 1985, pp. 669-677.

[4] Eggers, J. M., "Velocity Profiles and Eddy viscosity Distributions Downstream of a Mach 2.22 Nozzle Exhausting to Quiescent Air," NASA TN D-3601, September 1966

[5] Chien, K. Y., "Predictions of Channel and Boundary-Layer Flows with a Low-Reynolds-Number Turbulence Model," AIAA Journal, Vol. 20, No. 1, 1982, pp. 33-38.

[6] Menter, F. R., "Two-Equation Eddy-Viscosity Turbulence Models for Engineering Applications," AIAA J., Vol. 32, No. 8, August 1994, pp. 1598-1605.

[7] Spalart, P. R. and Allmaras, S. R, "A One Equation Turbulence Model for Aerodynamic Flows," AIAA Paper 1992-0439, 1992.

[8] Wray, T. J. and Agarwal, R. K., "A New Low Reynolds Number One Equation Turbulence Model Based on a k-ω Closure," AIAA Journal, Vol. 58, No. 8, pp. 2216-2227.

[9] Yang, Z. and Shih, T.H., "New Time Scale Based Model for Near-Wall Turbulence," AIAA Journal, Vol.31, No.7, 1993, pp.1191-1197.

[10] Launder, B. E. and and Sharma, B. I., "Application of the Energy Dissipation Model of Turbulence to the Calculation of Flow Near a Spinning Disc," Letters in Heat and Mass Transfer, Vol. 1, No. 2, 1974, pp. 131-138.

[11] Abid R., " Evaluation of Two-Equation Turbulence Models for Predicting Transitional flows," Int. J. Eng Sci, Vol.31, 1993, pp.831–40.

[12] Sarkar, S., Erlebacher, G., Hussaini, M. Y., and Kreiss, H. O., "The Analysis and Modelling of Dilatational Terms in Compressible Turbulence," Journal of Fluid Mechanics, 1991. Vol. 227, pp. 473-493.

[13] Wilcox, D. C. "Dilatation-Dissipation Corrections for Advanced Turbulence Models," AIAA J. Vol. 30, 1992, pp. 2639–2646.

[14] ANSYS® Fluent, Release 15.0, Help System, Theory Guide, ANSYS, Inc.

[15] Suzen, Y. B. and Hoffmann, K. A., "Investigation of Supersonic Jet Exhaust Flow by One- and Two-Equation Turbulence Models," AIAA Paper 98-0322, 36th AIAA Aerospace Sciences Meeting, Reno, Nevada, 1998.

[16] Carter, M. B., Elmiligui, A. A., Campbell, R. L., and Nayani, S. N., "USM3D Prediction of Supersonic Nozzle Flow," 32nd AIAA Applied Aerodynamics Conference, 2014.

[17] Gross, N., Blaisdell, G.A., and Lyrintzis, A.S., "Analysis of Modified Compressibility Corrections for Turbulence Models," AIAA Paper 2011-279, 2011.

[18] Pandya, M.J., Abdol-Hamid, K.S., and Frink, N. T.: "Enhancement of USM3D Unstructured Flow Solver for High-Speed High-Temperature Shear Flows." AIAA 2009-1329, January 2009.

[19] M. M. Rahman, T. Siikonen, and R. K. Agarwal. "Improved Low-Reynolds-Number One-Equation Turbulence Model," AIAA Journal, Vol. 49, No. 4, 2011, pp. 735-747.

[20] Shoemaker, J. "Performance of Seven Semicircular Lift-Producing Nozzles," NASA TN D-2731, 1965.

Vita

Han Ju Lee

701 limit Ave 2S, University City, MO 63130 | 314-570-5707 | hanjulee@@wustl.edu

Education

Washington University in St. Louis — Expected to Graduate: Summer 2017
BS/MS Aerospace Engineering — 3.80 Overall GPA /3.91 Major GPA

Honors and Awards

2016	Tau Beta Pi Engineering Honor Society
2015	Pi Tau Sigma Mechanical Engineering Honorary
2015	Summer Undergraduate Research Award
2010-2016	6 Dean's list

Research Experience

Graduate Researcher
Turbulence model research, Advisor: Dr. Agarwal — *Washington University in St. Louis*
Fall 2016- SP2017

- Developed a compressibility correction for Wray Agarwal(WA) turbulence model
- Coded the correction into ANSYS Fluent using C language based user defined function
- Demonstrated the correction for WA model performs better than other compressibility correction forms in the literature by performing both 2D and 3D supersonic jet flow simulations
- Script in preparation for submission at AIAA SciTech 2018

Undergraduate Researcher
Supersonic Nozzle CFD Research, Advisor: Dr. Agarwal — *Washington University in St. Louis*
Fall 2014- SP2016

- Built 2D axi-symmetric hybrid meshes using ANSYS ICEM
- Applied various realistic boundary conditions and simulated supersonic jet cases using ANSYS Fluent
- Studied two supersonic nozzle configurations and analyzed an ability of various turbulence models to capture the compressibility effect at high Mach number in the plume with multiple shock cells using ICEM and ANSYS FLUENT

Publications

- **Hanju Lee**, Tim Wray, and Ramesh K. Agarwal. "CFD Performance of Turbulence Models for Flow from Supersonic Nozzle Exhausts", 34th AIAA Applied Aerodynamics Conference, AIAA Aviation, (AIAA 2016-3433)
- **Lee, Han Ju**; Strahan, Nick; and Boyd, Emily, "Turbocharger Jet Engine Build and Engineering Analysis" (2016). *Mechanical Engineering and Materials Science Independent Study.* Paper 13.

Presentations

- **CFD Performance of Turbulence Models for Flow from Supersonic Nozzle Exhausts,** Han Ju Lee, Tim Wray and Ramesh K. Agarwal, 34th AIAA Applied Aerodynamics Conference; 2016 June 14, Washington D.C.

- **CFD Performance of Turbulence Models for Flow from Supersonic Nozzle Exhausts,** Han Ju Lee, Tim Wray and Ramesh K. Agarwal, Poster session presented at : Washington University in St. Louis Undergraduate Research Symposium; 2016 Oct 29; St. Louis, MO